Optimization of CVT control for hybrid and conventional drive lines

Oudijk, M.F.

Award date:
2005

Optimization of CVT control

For Hybrid and Conventional drive lines

M.F. Oudijk

Report no: DCT-2005-140

TU/e Master Thesis Report
21st November 2005

Supervisors:
dr. ir. B.G. Vroemen (TU/e)
Prof. dr. A.A. Frank M.Sc. Ph.D.(UC Davis)
ir. J.H.M. van Rooij (GCI)
ir. J.H. Nelissen (GCI)

Master Thesis committee:
Prof. dr. ir. M. Steinbuch (chairman)
dr. ir. B.G. Vroemen
ir. J.H.M. van Rooij
dr. ir. W.J.A.E.M. Post

Eindhoven University of Technology
Department of Mechanical Engineering
Division Dynamical Systems Design
Master track Automotive Engineering Science

University of California, Davis
Department of Mechanical Engineering
Hybrid Electric Vehicle Center
Gear Chain Industrial B.V.

Summary

The University of California in Davis has built a parallel, battery dominant, plug-in hybrid-vehicle. To fully utilize the possibilities of this hybrid power train it is decided to replace the manual transmission by a Continuously Variable Transmission. This required a new type of transmission to be designed and to renew the power train controller for the vehicle. The CVT is actuated with a servo-hydraulic actuation system. To gain experience with this actuation system it has been implemented in a vehicle.

The first chapter of this report discusses different types of hybrid vehicles in general and the hybrid vehicle built by UC-Davis in more detail. It is explained why certain decisions are made which have led to the current configuration. The next step in the development of this hybrid vehicle is the replacement of the manual transmission by a CVT. The advantages of a CVT as well as the required power train controller are discussed. The second chapter handles the new type of transmission, the inline CVT, which is designed for this vehicle. The characteristic behavior and the differences with a conventional CVT are explained. The inline CVT is actuated with a servo-hydraulic actuation system, since this system is expected to use less power to actuate the CVT compared to a conventional actuation system. The theory of this system is discussed in chapter three. To gain experience with the actuation system it is built into a stock vehicle. What is needed and how this is done is explained in chapter four. Finally, the model derived in the previous chapter is compared with measurements done on the vehicle.

Contents

Introduction

The University of California in Davis is working on a project to build a hybrid vehicle with a Continuously Variable Transmission. This thesis discusses the implementation of an improved actuation and control system for CVTs in hybrid and conventional drive lines.

First a brief introduction about hybrid vehicles in general will be given. Different types of hybrids are discussed. The parallel, battery dominant, plug-in hybrid-vehicle designed and built by the Hybrid Electric Vehicle center of the University of California in Davis will be discussed in more detail and the advantage of a CVT for this vehicle will be shown. To be able to implement a CVT in this vehicle two issues had to be solved. First of all, a new power train controller had to be designed to control the CVT power train. The second issue was realizing a new type of CVT, the inline CVT, which could be placed into the vehicle. Two prototypes were realized and the specific behavior of this inline-CVT is discussed.

To control the inline-CVT a servo-hydraulic actuation system is chosen. The servo system has been connected to the CVT and it is shown that the concept of the inline-CVT works.

A model of the servo actuation system is made which is used to analyze the dynamic behavior and the expected power consumption.

To verify the model of the servo system and to gain experience with this system in a vehicle it was chosen to build it into an actual car. A Volvo-440 is chosen for this purpose since the hybrid vehicle was no longer available. All modifications to the vehicle to be able to implement the system are discussed and measurements are done on the system to verify the model. Problems which occurred during the implementation are discussed and solved and recommendations are made for future projects.

The first part of this project has been performed under supervision of professor Andrew A. Frank, head of the HEV center of the University of California, where I have worked for half a year. During that period I focused on the design of a power train controller for a hybrid vehicle with a CVT. Besides that the inline CVT has been realized and presented at the International Continuously Variable and Hybrid Transmission Congress 2004 organized by prof. Frank. The inline CVT is a cooperation between UC-Davis, Gear Chain Industrial B.V. and A.W. Brown Co.Inc. After my stay in California I continued the project at Gear Chain Industrial B.V. in Nuenen where I implemented the servo-hydraulic actuation system in a real vehicle.

Chapter 1

Hybrid Electric Vehicles

A hybrid vehicle is a vehicle with different types of power sources. In this report only electric hybrids are considered. This means there is a power source based on fuel (this can be gasoline, hydrogen or something else) and an other source based on electricity. Usually the fuel has to be tanked, the electricity can be received either from the grid (plug-in hybrids) or can be generated by the vehicle itself.

Hybrids can be divided into two different configurations: series and parallel hybrids. The series configuration has no mechanical connection between the engine and the wheels. The wheels are driven by a motor, which is electrically powered (see figure 1.1). Very often the motor can also be used as a generator to recover braking energy. The electric power is supplied by an engine driven generator in combination with a battery or capacitors. The engine only has to deliver the power used on average over a period of time, the battery will assist during an acceleration and will recover some of that power again when braking. A big advantage of a series hybrid is that the engine can be operated at one point, which has the best power to fuel consumption ratio and the engine can be specifically designed for this operating point. The biggest disadvantage is that there will always be a conversion from mechanical energy to electrical energy and back to mechanical energy again which will decrease the overall efficiency. Examples of series-hybrids are the TNO Volkswagen Beetle and the Phileas bus.

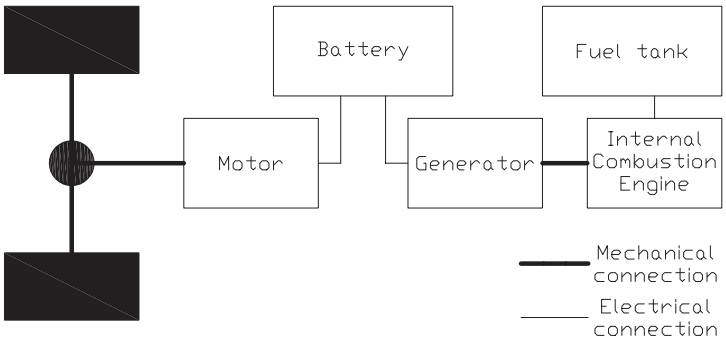

Figure 1.1: A series hybrid power train

In a parallel configuration, there is a direct link between the engine and the wheels but also between the electric motor and the wheels as can be seen in figure 1.2. Both devices can deliver power to the wheels and the motor can also be used as a generator again to recover energy when braking. By means of different couplings the vehicle can be driven all electric or the batteries can be charged by the engine. The advantage of this configuration is that there is no unnecessary conversion from mechanical power to electrical power, whereas the disadvantage is that the engine cannot be designed specifically for one single operating point. However, it is possible to use the engine on the ideal operating line. There are parallel hybrids, which use a relatively small motor to deliver a power assist, but these hybrids cannot operate solely on the electric motor. Parallel hybrids that can be driven on electricity only can be divided into two groups. The first group can be used as an electric vehicle, because there is a large battery pack present. The second group can only take off on the electric motor, the engine has to be used as soon as the vehicle is moving.

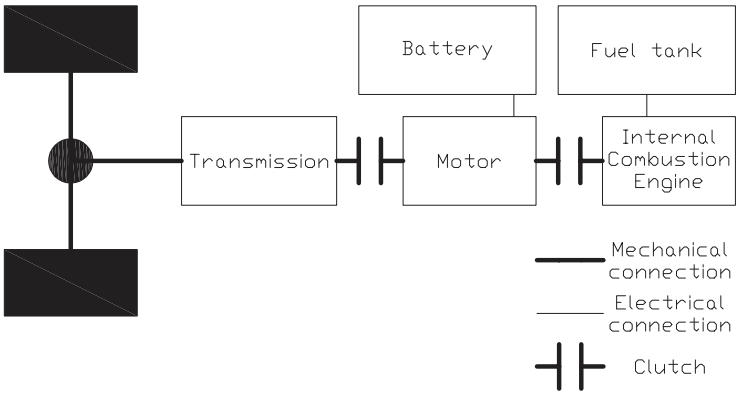

Figure 1.2: A parallel hybrid power train

Besides these two clear configurations, there are many combinations possible, called dual

hybrids (figure 1.3. The Toyota Prius for example uses a power-split device, which can transfer the power from the engine to the wheels and to a generator. A big disadvantage of this type of system is the complexity caused by the need of two electric machines. The power train of the Prius is shown in figure 1.4

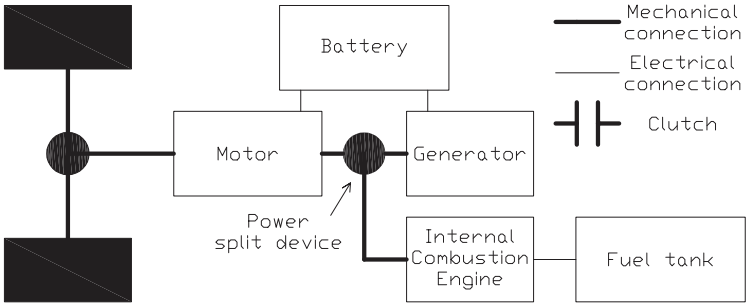

Figure 1.3: A dual hybrid power train

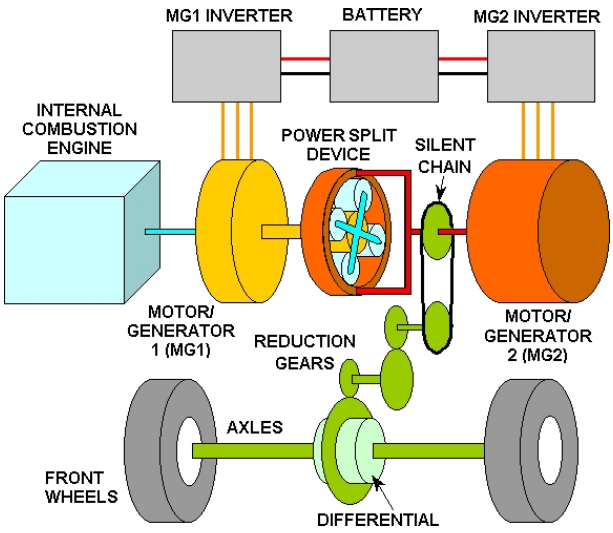

Figure 1.4: The Toyota Prius power train

1.1 Yosemite: the UC-Davis HEV-center hybrid vehicle

One example of a parallel hybrid is Yosemite, built by the Hybrid Electric Vehicle Center (HEV Center) at the University of California, Davis. The HEV Center has been working with battery dominant hybrid vehicles for over 10 years. These are electric hybrids in

which the battery is dominant compared to the combustion engine. With recent focus on sports utility vehicles (SUVs), the HEV Center has designed and developed a parallel hybrid vehicle built on a Ford Explorer U152 platform. In figure 1.5 Yosemite is shown at the 2004 Future Truck competition at the Ford Proving Grounds in Dearborn, Michigan

Figure 1.5: Yosemite at the 2004 Future Truck competition.

The design philosophy behind Yosemite is based on the idea to build a hybrid, which will fulfill Californian vehicle demands. This means it has to meet the following objectives:

- Maximize vehicle energy efficiency
- Minimize fuel consumption
- Reduce fuel cycle greenhouse gas emissions
- Achieve California Super Ultra Low Emission Vehicle (SULEV) target in city driving
- Deliver best-in-class performance

Yosemite is a parallel plug-in hybrid. A series hybrid configuration was not chosen because it requires chemical energy to be converted to electrical energy before it drives the wheels, resulting in unnecessary inefficient energy conversions. While a dual hybrid design has lower conversion losses than a series configuration, it is costly and mechanically more complex. A parallel hybrid configuration gives many advantages as well as more operating modes. The entire power train is built up with relatively simple parts connected in an intelligent way. Since Yosemite is a plug-in hybrid, it is possible to operate it in an electric vehicle mode (EV) as well as in a hybrid electric vehicle mode (HEV). The EV-mode is

only possible since Yosemite is a plug-in hybrid, which means it can charge its battery pack from the grid. The EV-mode is especially useful for short city trips. In EV-mode the vehicle has no emissions at all which, in some polluted cities, is a very big advantage. Of course the electricity has to be generated somewhere, but because of the very large scale on which this can be done as well as the fact that the location where it is generated can be chosen it is easier to control the well-to-tank emissions (WTT) in this situation. The tank-to-wheel emissions (TTW) depend on the driving strategy and the total well-to-wheel emission (WTW) can thereby be influenced a lot. Of course the WTW depends on the type of fuel which is used and on the path which is chosen to create the fuel (both gasoline and electricity). It is shown that in general the WTW of electricity is better compared to most types of gasoline [W+01].

A plug-in hybrid can only be used if the user has the possibility to connect the vehicle to the grid. In American suburbs where people have a private parking lot or on large company parking lots this will not be a problem, the United States Postal for example is performing a pilot project to charge some of their vehicles over night. In many European and Asian cities however, it may not be possible to charge a vehicle from the grid since people do not have their own parking lot. Yosemite can also operate in a HEV-mode. In the HEV-mode the vehicle operates as a real hybrid in which the combustion engine and the electric motor work together to drive the vehicle. There are two ways to operate the vehicle in the HEV-mode. A charge depleting mode (CD) and a charge sustaining (CS) mode. The charge depleting mode uses both the electric motor and the combustion engine, but the state of charge (SOC) of the battery will be depleted during the ride. Again, this mode is only possible since Yosemite is a plug-in hybrid. The advantage of the CD-mode compared to the EV-mode is the increase of the range of the vehicle. When the total driving distance is known in advance it is possible to optimize the fuel consumption and emissions especially for that trip. The other mode is the CS-mode, when the SOC of the battery drops below a certain level the vehicle will automatically switch to the charge sustaining mode. In this mode the SOC will remain the same over a period of time. This mode is the only mode which can be used when the vehicle is not operated as a plug-in hybrid but as a regular hybrid. It is also the most complex mode to control since a trade-off has to be made between fuel consumption, emissions (WTW or TTW), SOC and the efficiency of the battery and motor by the power train controller.

Yosemite was built to participate in the Future Truck 2004 competition. This is a competition between 15 American Universities, organized by the Department of Energy, Ford Motor Company and many other companies, to rebuild a Ford Explorer to achieve lower-emission and at least 25% higher fuel economy, without sacrificing the performance, utility, safety and affordability consumers want. This includes features such as cruise control, air conditioning and entertainment systems.

The internal combustion engine of Yosemite is sized to meet steady state highway driving conditions while the electric motor is used for low speed driving and transient conditions. Reducing the engine size allows the engine to operate at higher average thermal efficiency and within its ideal operating region, increasing fuel economy. To determine the required

capacity of the engine the road load (F_{RL}) for the vehicle in steady state conditions is determined. The running resistance (without acceleration forces) is determined by three different components: rolling resistance, aerodynamical drag and climbing resistance.

$$\begin{aligned} F_{RL} &= F_{rol} + F_{dra} + F_{sli} \qquad (1.1) \\ F_{rol} &= f_{rol}\, m\, g\, cos(\alpha_{road}) \\ F_{dra} &= 0.5\, \rho_{air}\, c_d\, A_{front}\, v^2 \\ F_{cli} &= m\, g\, sin(\alpha_{road}) \\ P_{RL} &= F_w\, v \qquad (1.2) \end{aligned}$$

In this equation, f_{rol} is a coefficient of rolling resistance, m is the total vehicle weight, g is the gravitational acceleration, ρ_{air} is the density of the air, c_d is a drag coefficient of the vehicle, A_{front} is the largest cross-section of the vehicle, v is the vehicle speed and P_{RL} is the power needed to overcome the steady state running resistance. Given the fact that the engine has to meet the maximum steady state conditions the power consumption is also calculated for highway driving with a slight hill-climb and a trailer which is added for extra weight. The result is shown in figure 1.6. The maximum power output of the engine has to be equal to the power consumption at a vehicle speed of 110 km/h (=70 mph) and is chosen to be 85 kW. The steady state power consumption for daily use (which means no trailer or hill-climb) is also shown.

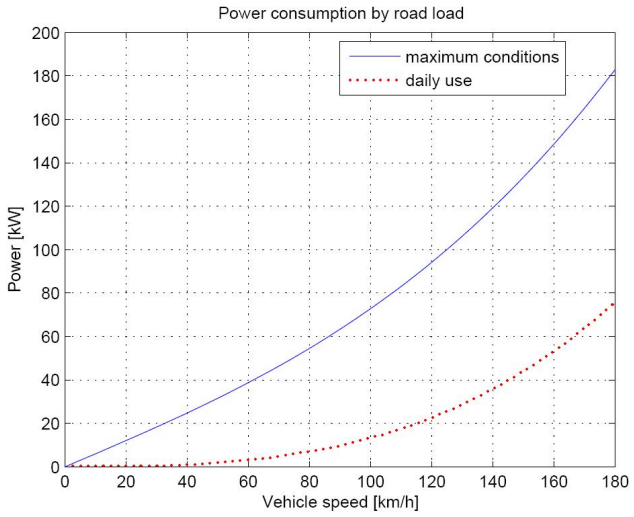

Figure 1.6: The power consumption of the road load for steady state conditions.

The electric motor has to be able to drive the vehicle at low speeds and is used for additional power during acceleration. This includes no additional trailer-towing or extreme hill-climbing, but the motor has to be able to accelerate the vehicle in an acceptable manner.

Based on these demands and availability an electric motor of 75 $\boldsymbol{kW}$ is used. The size of the battery pack is based on a study performed by the Electric Power Research Institute (EPRI) and Delphi, Dynamics and Propulsion Innovation Center, indicating that over 54% of US motorists drive 75 km or less daily [BGM72]. When fully powered by the grid Yosemite has to be able to drive 75 km all-electric. The battery pack, which operates at a nominal voltage of 317 $\boldsymbol{V}$ has to have a capacity of 50 $\boldsymbol{Ahr}$ to meet these demands according to simulations run with ADVISOR and PSAT done by the HEV center [ABC$^+$04].

The given conditions result in the following power train specifications:

Internal Combustion Engine

- Type: 1.9 L Saturn
- Max power: 82 kW @ 5500 rpm
- max torque: 155 Nm @ 4500 rpm

Electric Motor

- Type: Permanent Magnet DC motor, UQM SR218N, Unique Mobility
- Max power: 75 kW @ 3000-8000 rpm
- Cont power: 35 kW @ 3000-8000 rpm
- Max torque: 240 Nm @ 0-3000 rpm
- Cont torque: 110 Nm @ 0-3000 rpm
- Max speed: 8000 rpm

Battery pack (NiMH)

- energy density: 55 Whrs/kg
- power density: 750 W/kg
- Capacity: 50 Ahr
- Operating voltage: 317 V

It has to be taken into account that the valued mentioned here are peak values. For the durability of the battery pack it will be better to use a power density of approximately $\boldsymbol{150W/kg}$.

In addition to the major power train adjustments described here several other adjustments have been made compared to the stock vehicle like throttle controllers, clutch controllers etc.

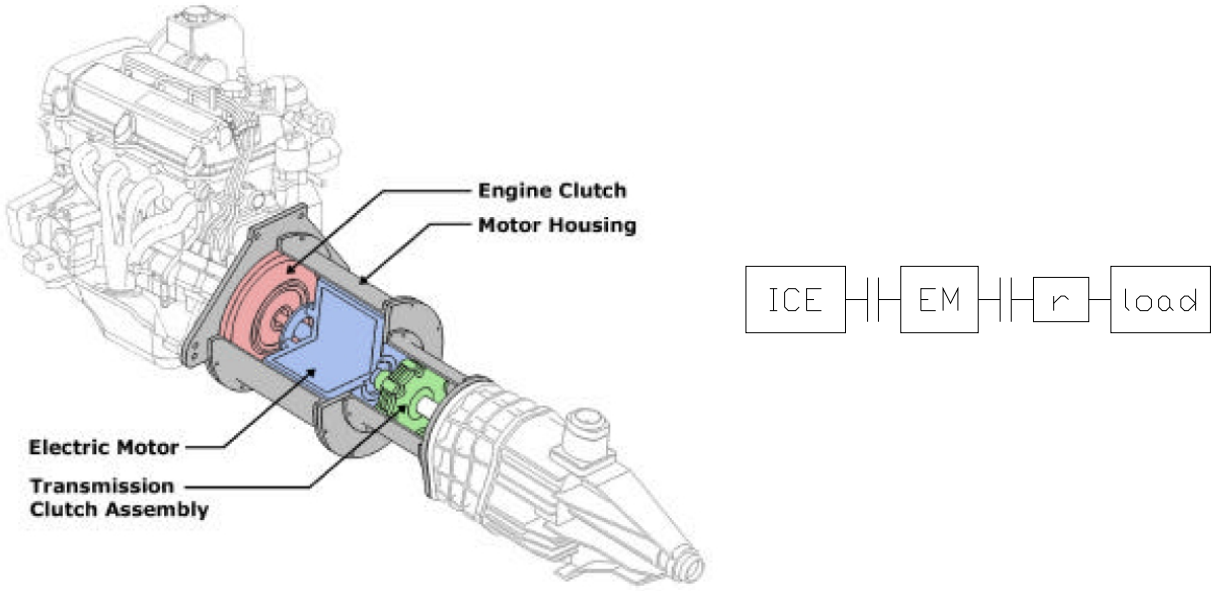

Figure 1.7: The current upgraded power train of Yosemite.

In figure 1.7 the upgraded power train of Yosemite can be seen. The new smaller engine (left) is connected to the manual transmission (right) by the electric motor housing. The motor housing contains three parts. The first part is the engine clutch, which is used to decouple the engine, the second and most important part is the electric motor itself. This is a specially designed motor with a through-shaft. The last part is the transmission clutch, which is used to decouple the power sources when shifting.

With the new power train lay-out the vehicle can be used in EV- and HEV-mode. In the EV-mode the vehicle has a range of about 75 km. This mode is especially useful for short city-trips and should be manually chosen since it is not possible to detect the distance that is going to be traveled in advance. In the HEV-mode the engine will be turned on and off while driving depending on vehicle speed and the SOC of the battery pack and thus expanding the vehicle range. As long as the SOC is above 20 % the power train will operate relatively efficient depending on expected driving distance. When the SOC reaches 20 % the controller has to switch strategies. It is necessary to maintain a certain energy level since this is needed for a take-off of the vehicle. The engine will be used more compared to the CD-strategy to ensure the SOC will not become too low. Over a longer period of time the SOC will remain constant so the engine will be charging the batteries a little when driving. Since the combination of engine and motor in CS HEV-mode is more complex in comparison with the EV-mode, the power train controller for this mode will be discussed in section 1.2.

1.1.1 Implementing a CVT in a hybrid power train

To fully utilize the possibilities of the upgraded power train it is required to use a CVT instead of the current manual transmission. At this moment, a LED tells the driver when it is necessary to shift up or down. The current gear is compared with a higher and a lower gear and when an other gear is more efficient this is shown to the driver. The disadvantage of this system is that it is up to the driver to shift or not and only a few discrete operating points can be chosen due to the characteristics of the manual transmission. A CVT will shift automatically and can do this continuously thus improving the overall performance. By replacing the current transmission with a CVT a controller completely takes over the shifting strategy and the speed and torque of the engine and motor are completely decoupled from the wheels. Basically, the entire system with a CVT has only one user input (throttle pedal) and can be optimized completely towards emissions, fuel consumption, performance or any combination of those items. This gives a lot of extra possibilities to design a control strategy that can be optimized in many different ways. Initially the high-level power train controller will be focused on reducing fuel consumption. In the future, certain emissions or other aspects can also be taken into account.

At this moment, the only CVT available that can transfer the required torque is the GCI Medium Duty CVT. A custom design based on this transmission has been made where the input and output shaft are concentric. This CVT will be discussed in chapter 2. Besides changing the transmission some sophisticated control hardware has to be used to be able to control all the different parts in the power train. This controller will be used to run the power train controller as well as the low-level CVT controller. The low-level CVT controller controls the CVT itself (ratio and clamping pressure) whereas a high-level CVT controller sets the desired ratio and transmittable torque. The high-level CVT controller is usually integrated into the power train controller which also determines engine- and motor speed and the (dis)engagements of clutches. The low-level clutch- and throttle controllers will not be adjusted, since they already operate in the current vehicle with the manual transmission.

1.2 Hybrid Electric Vehicle controller

The only way the technologies used in this prototype will ever be implemented in commercially available vehicles, is when the performances as well as the drivability of a standard vehicle are matched while fuel consumption and emissions are improved, all without any major additional costs. This is the idea of the Future Truck competition.

1.2.1 User input

Due to the performance demand pressing the accelerator pedal should result in a direct acceleration. It is decided to interpret the pedal command as a command to the wheels,

i.e., power train dynamics should not influence the final vehicle response. By modeling the power train dynamics all parasitic effects can be compensated for by the power train controller as long as saturations are not encountered.

Depending on the vehicle speed the accelerator pedal will be interpreted as a torque or as a power request at the wheels. A power request is closest to a conventional vehicle. In figure 1.8 the road load in torque and power at the wheels is given. It can be seen that if the pedal position is interpreted as a power request the change in vehicle speed due to a change in pedal position will be smaller then if it would be a torque request for higher vehicle speed. This feels much more natural.

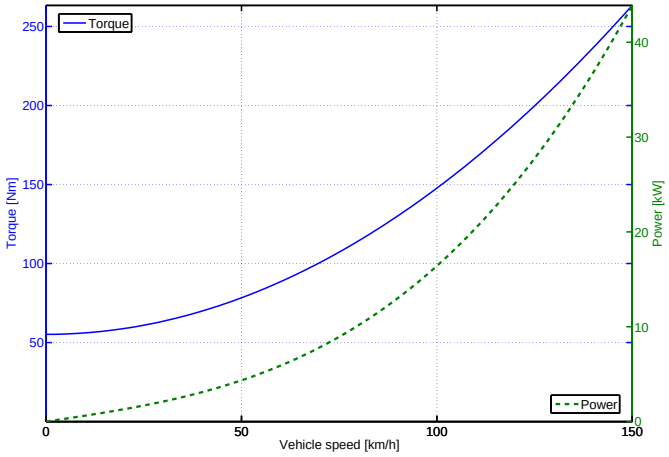

Figure 1.8: The road load given as power and torque at the wheels.

At low speed however a power request is undesirable, because this would result in a very high torque or even an infinite torque request at zero speed. Even though infinite torque could never be generated by the motor the maximum torque would be fully utilized when taking off which will result in a very poor drivability. Due to the limited traction capabilities the wheels would always slip when taking off. Therefore, at low vehicle speed, the pedal position is translated into a torque request, which transfers to a power request at higher speed. To prevent a torque jerk when transferring from the torque-zone to the power-zone the transition should be continuous. This means that, given a certain pedal position, the torque request is constant below the transition speed. When the vehicle reaches the transition speed the power-request will continue along a constant-power line. Due to the large ratio range of the inline CVT, the maximum power of the hybrid power train is available at a very large speed range. At very low speeds the maximum available power drops because the ICE cannot be used.

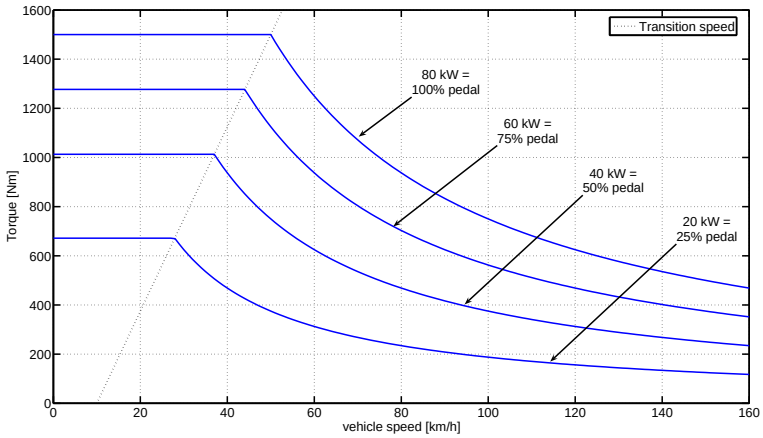

Figure 1.9: Requested torque for given vehicle speed and throttle pedal.

1.2.2 Engine, motor and ratio set point

Since a CVT makes it possible to decouple torque at the wheels from torque generated by the engine and motor, these devices only have to deliver a certain power. Within the limitations of the ratio range the combination of engine and motor can operate in the most efficient way possible. This makes it possible to operate the engine in a very specific way. The engine used in this vehicle has been tested on a dynamometer. The engine map generated by these tests has been converted to a look-up table and used in the power train controller. It would be possible to use a torque transducer to know the torque more accurately, but these transducers are too expensive to ever be implemented in commercial vehicles. Depending on the optimization parameters, different engine maps will be used. This can be a fuel consumption map or different kinds of emission maps. For the electric motor only an efficiency map is used (both in motor and generator mode). Only fuel consumption will be discussed here [Fra04a].

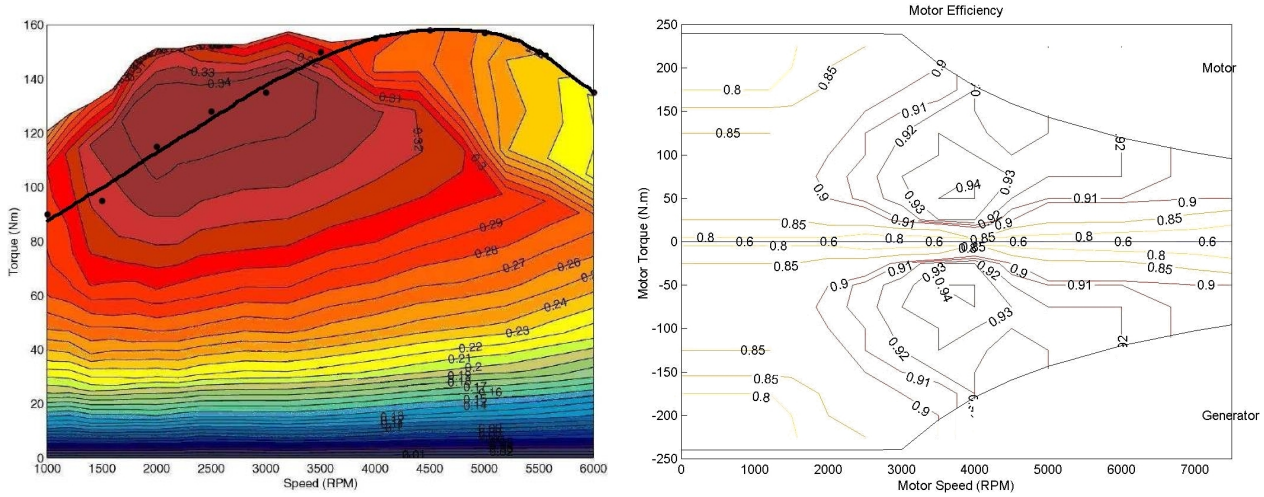

(a) The engine map with the Ideal Operating Line.

(b) The efficiency map of the electric motor.

Figure 1.10: Engine and motor map

When there is a positive power flow (motor and engine are delivering power to the vehicle) the engine will be operated on the Ideal Operating Line (IOL). This is a smooth line through all the points which represent the torque and speed combinations at which the fuel consumption is minimal on different power lines for steady state conditions (see figure 1.10(a)). The IOL is also known as the e-line. It is also possible to use an IOL, which is not based on fuel consumption but on other parameters like different types of emissions. The efficiency of the electric motor (as a motor, not as a generator) has also been tested, as shown in figure 1.10(b). It can be seen that the motor has an optimum operating zone in the motor-mode, the generator-mode is considered symmetric to the motor-mode as long as no measurements are available. When the accelerator pedal is pushed down the power request increases (from point A to B in figure 1.11) for example from $\mathbf{20}\boldsymbol{kW}$ to $\mathbf{50}\boldsymbol{kW}$. The instantaneous power will be delivered by the motor (B). Then the CVT will start to shift the engine along the IOL to the new operating point (C). While the engine speed increases (and thus the engine power increases) the power delivered by the motor will decrease accordingly. The power delivered by the motor is filled black in figure 1.11.

The time in which the engine speeds up from the first operating point A to the second one C determines how much energy the battery has to deliver. However, it is not advisable to shift too fast. First of all, there is a physical limitation on how fast the CVT can shift. More important is the influence of the change of ratio to the torque at the wheels.

In a regular transmission both the primary and secondary inertias ($\boldsymbol{J_1}$ and $\boldsymbol{J_2}$) can be seen as vehicle weight. When shifting to an other gear the equivalent mass of the vehicle will change, but the vehicle will respond in the same way every time the transmission is in a certain gear. With a CVT the vehicle response (here the torque at the drive shaft) depends on the ratio $\boldsymbol{r}$ as well as the ratio rate $\boldsymbol{\dot{r}}$. This is shown in equation 1.5. The derivative of

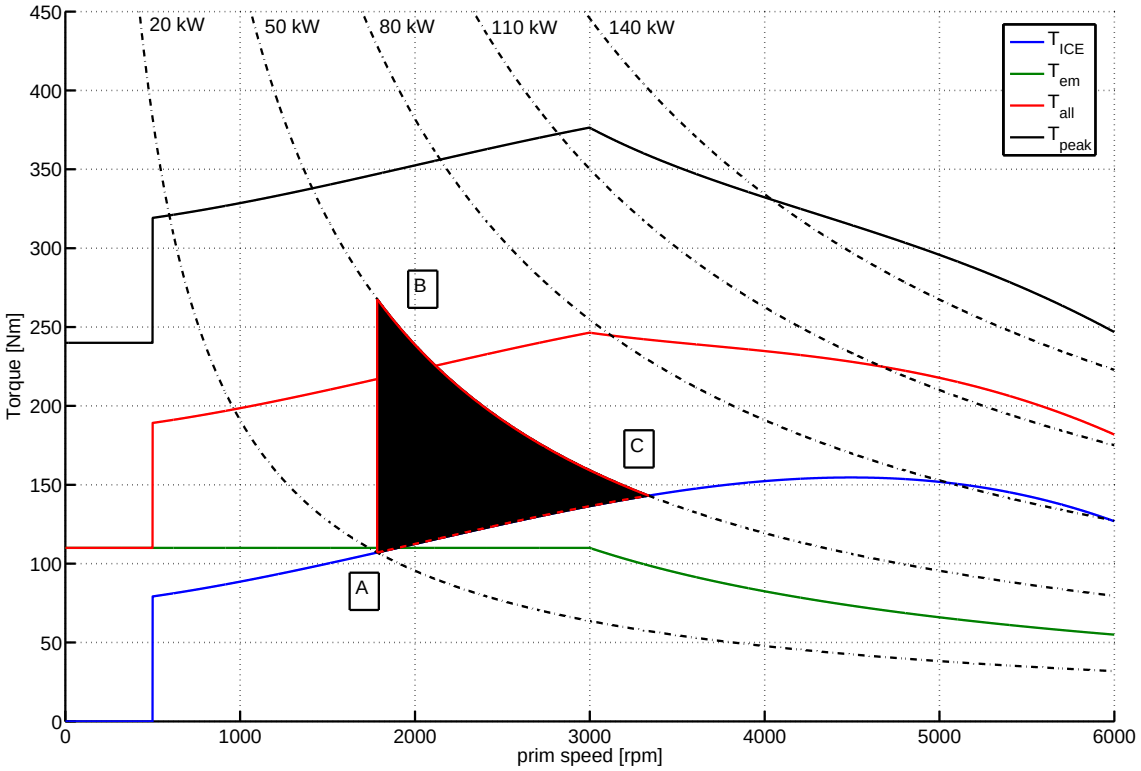

Figure 1.11: Acceleration and shifting sequence

the primary speed (equation 1.3) is substituted in Newton's law describing the drive train (1.4).

$$\begin{aligned} r &= \frac{\omega_2}{\omega_1} \rightarrow \\ \dot{\omega}_1 &= \frac{\dot{\omega_2}}{r} - \frac{\omega_2\,\dot{r}}{r^2} \end{aligned} \tag{1.3}$$

$$(T_{EM} + T_{ICE}) - r\,T_{drive-shaft} = J_1\,\dot{\omega}_1 + r\,J_2\dot{\omega}_2 \tag{1.4}$$

$$\begin{aligned} T_{drive-shaft} &= \frac{(T_{EM} + T_{ICE})}{r} - \frac{J_1\,\dot{\omega}_1}{r} - J_2\,\dot{\omega}_2 \\ T_{drive-shaft} &= \frac{(T_{EM} + T_{ICE})}{r} - \frac{J_1\,\dot{\omega}_2}{r^2} + \frac{J_1\,\omega_2\,\dot{r}}{r^3} - J_2\,\dot{\omega}_2 \end{aligned} \tag{1.5}$$

In figure 1.12 the vehicle speed is shown during an acceleration action. The engine torque increases from $\mathbf{10}\boldsymbol{Nm}$ to $\mathbf{120}\boldsymbol{Nm}$ on $\boldsymbol{t} = \mathbf{1}\boldsymbol{sec}$ and transmission shifts in an extreem manner from HIGH to LOW ratio in $\mathbf{0.1}\boldsymbol{sec}$. It can be seen that the vehicle slows down initially before it accelerates.

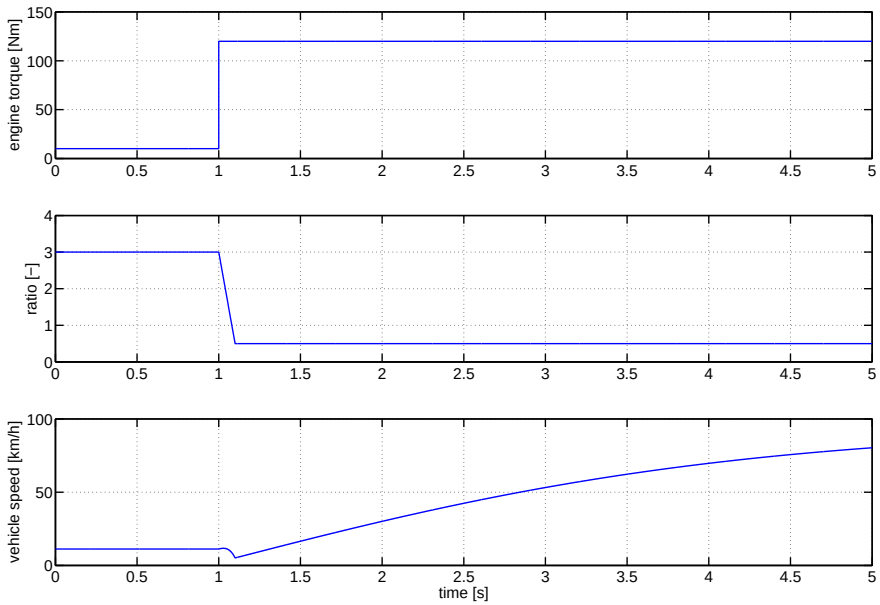

Figure 1.12: The influence of an extreem $\dot{r}$ on the acceleration of a vehicle

As mentioned before the user of the vehicle should not notice anything from the power train dynamics. The drop in available torque at the wheels due to the $\dot{r}$ term has to be compensated for by the motor. The maximum motor torque, the efficiency of this motor, the IOL of the engine and the SOC of the battery will determine how long it will take to speed up the engine to the new operating point. At this moment a first order time-constant is used to transfer from one operating point to an other in the power train model. Measurements of the energy consumption, efficiency and shift rates have to determine what kind of algorithm has to be used in order to maintain the demanded SOC. To ensure the drivability demands this ratio set point will be clipped when the ratio rate will become too high to be compensated for by the electric motor.

When there is a negative power flow, during a brake action, the CVT will shift in such a way that the efficiency of the electric motor (which operates as a generator at that moment) will be as high as possible. To prevent an energy flow from the engine to the batteries the engine is decoupled.

1.2.3 Controller lay-out

The strategy discussed is implemented in a power train controller. This controller consists of an engine-, a motor-, a clutch- and a CVT controller as can be seen in figure 1.13 (blue blocks). To be able to test this controller a very simple vehicle model (red blocks) has been built in Matlab/Simulink. Simulation results show that the power train controller is able to create the necessary set points for the hybrid power train. As soon as some real data of the

CVT that will be used for the hybrid power train is present additional simulations in PSAT and ADVISOR can be done by the HEV-center to predict the possibilities of additional fuel reduction and to create more efficient controller algorithms for the different controllers for optimal performance. PSAT ('Powertrain System Analysis Toolkit') is a forward facing vehicle simulation toolkit developed by Argonne National Laboratory. A forward facing simulation is very suitable to test control algorithms. ADVISOR is a backward facing tool used to perform vehicle systems trade-off analyses and to optimize fuel economy and minimize emissions [Lab01].

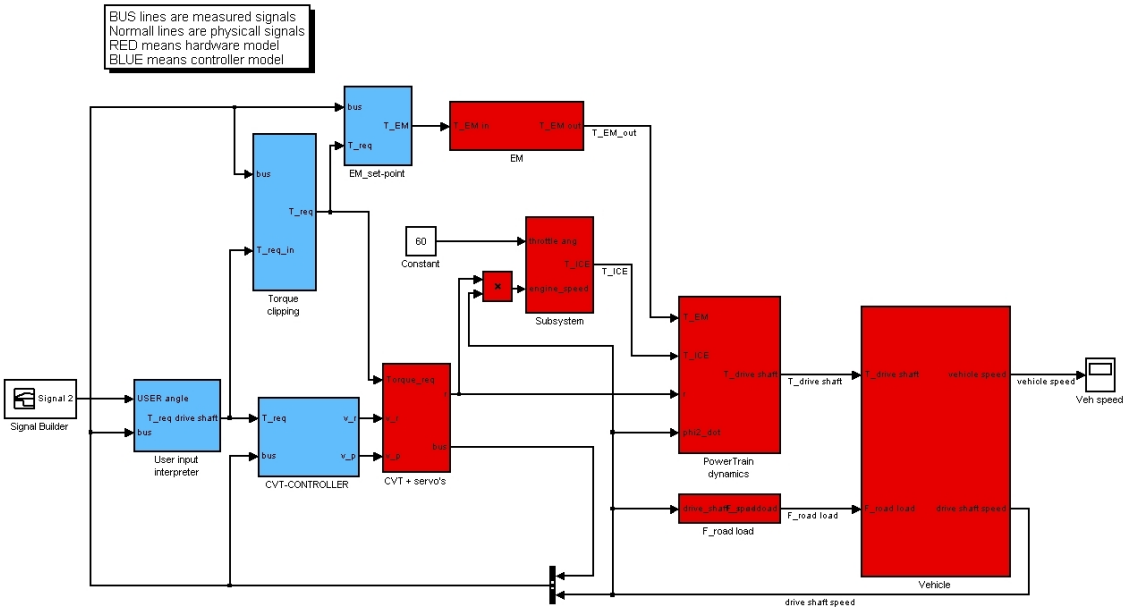

Figure 1.13: The power train controller, which can be used in PSAT with a simple vehicle model

Chapter 2

The Inline CVT

Because there is currently no CVT available that can be used as a direct replacement for transmissions in rear wheel driven SUVs or small trucks, UC-Davis and GCI developed a new concept [Fra04b] for a CVT . This inline CVT is capable of transmitting 500 Nm input torque and the input and output shaft lay inline. The first prototype is built and shown at the 2004 International Continuously Variable and Hybrid Transmission Congress [FBvR04].

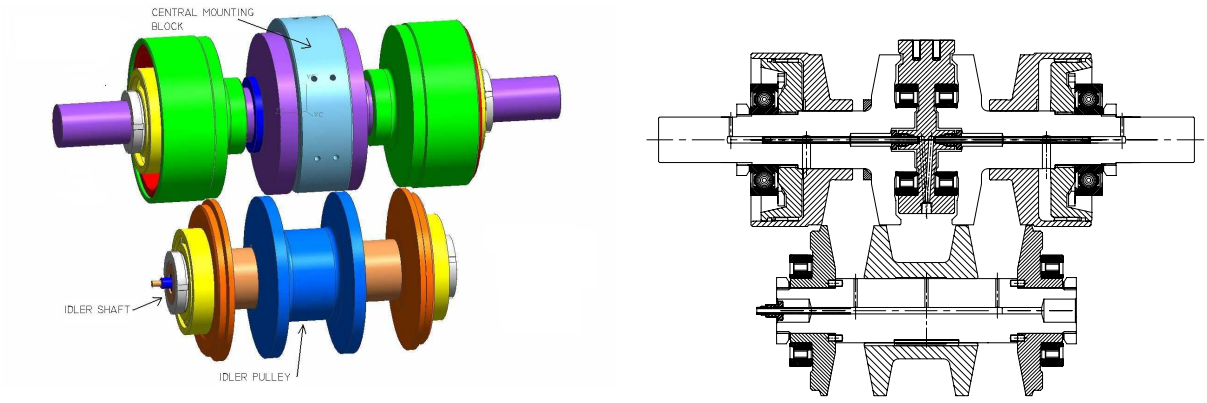

Figure 2.1: A side view and a section cut of the inline CVT

The inline CVT is principally based on two conventional CVTs, which are placed in series. The output pulley of the first CVT is connected to the input pulley of the second one. This means that the input pulley of the first CVT is the primary pulley of the inline CVT. The primary pulley is the pulley connected to the primary drive train, thus to the combustion engine or to the electric motor. The output pulley of the first CVT is an idler pulley. This means this pulley will not be actively actuated. The input pulley of the second CVT is also an idler pulley. These two pulleys are integrated on one shaft, the idler shaft. The output pulley of the second CVT is the secondary pulley which means it is connected to the secondary drive train and to the wheels by the drive shaft and the differential. Actuation

of the CVT will be done by pressurizing only two pulleys, the primary and the secondary. The primary pulley will be used to control the ratio and the secondary pulley to control the clamping forces and thereby the transmittable torque.

All the axial forces in the idler shaft are balanced and the idler shaft will not execute large axial forces on the housing of the CVT. However, the idler shaft will move a little bit in axial direction when shifting. This might introduce some very small forces into the housing. The movement is caused by the misalignment of the chain during shifting [Bra03]. To make this movement possible two roller-bearings (in stead of ball-bearings) are used to keep the shaft in position. These bearings allow small axial movement and will have to compensate for the radial forces working on the shaft caused by the two chains. The primary and secondary pulley are both hold in position by one ball-bearing and one roller-bearing to prevent these pulleys from being over constrained. Again there will be no force working in axial direction, only in radial direction. All these forces are led through the housing of the CVT and will not be led into the vehicle.

The movable sheave on the intermediate shaft is fixed to the shaft in tangential direction. Because there will always be some micro slip between pulley and chain it can happen that the movable sheave would rotate a bit faster or slower than the fixed sheave and the shaft. This could create unwanted torques or vibrations between chains, shaft and pulleys. To prevent this, a key has been placed between shaft and movable sheave to prevent a relative angular movement from the sheave compared to the shaft. This key will make it harder for the sheave to move in axial direction, however the shift rates are relatively slow and the clamping forces very high, so the moving sheave can easily overcome the friction caused by this key.

The actuation of the inline CVT can be done similar to a conventional CVT. It is chosen to use a servo-hydraulic system because of the reduced power consumption of this system. This system will be discussed in chapter 3. The pressure for both actuated pulleys is connected to the central mounting block. A narrow tube with a very small tolerance is fixed to the mounting block and placed concentric with the fixed shaft (see figure 2.2. The leakage between tube and shaft and at the end of the tube will operate as lubrication.

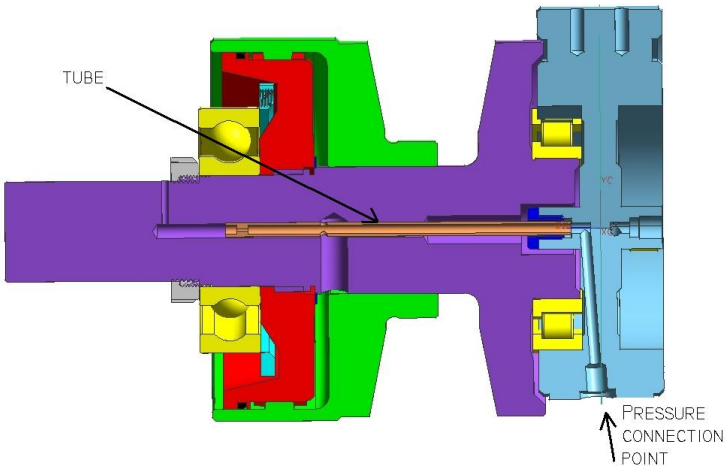

Figure 2.2: One of the tubes to actuate the CVT

2.1 Assembly

After production of the parts for a first prototype some minor adjustments were made before everything was assembled. There were two difficulties expected to occur during the assembly. The first one was to assemble the entire idler shaft. The two fixed sheaves on the idle shaft are fixed to the shaft with 16 spring pins (see figure 2.3. These are pins that can flex a little bit, allowing the sheave to rotate slightly relative to the shaft to prevent an over restrained situation. These pins realize a force-closed positioning in stead of a form-closed. To put the shaft and the sheaves together the center hole in the pulley has to become $\mathbf{0.018}\boldsymbol{mm}$ larger compared to the shaft, which has a diameter of $\mathbf{45}\boldsymbol{mm}$. This is done by heating the pulley in an oven and cooling the shaft with liquid nitrogen. Even though a temperature difference of only $\mathbf{30°}\boldsymbol{C}$ would be sufficient according to equation 2.1 it is decided to create a gap which is as big as possible so there is some time to align the 16 spring pins with the holes in the sheave. When the pins are aligned with the holes the sheave is further pressed on the shaft with a hydraulic press.

$$\boldsymbol{\Delta T} = \frac{\boldsymbol{\Delta D}}{\boldsymbol{\alpha_{steel} D_0}} \tag{2.1}$$

In this equation $\boldsymbol{\Delta T}$ is the created temperature difference, $\boldsymbol{\Delta D}$ is the change of diameter, $\boldsymbol{\alpha_{steel}}$ is the thermal expansion coefficient of steel and $\boldsymbol{D_0}$ is the original diameter.

The second expected problem was to put the chains around the pulleys when all pulleys were already assembled. It is undesirable to close the chain after it is wrapped around the pulleys, since this would require an unassembled chain to be be used. It is not possible to accurately close the chain anymore when it is already placed around the pulleys. Due to the two tubes that are placed into the primary and secondary pulley both pulleys have to be kept on the central mounting body the entire time during assembly. To make this

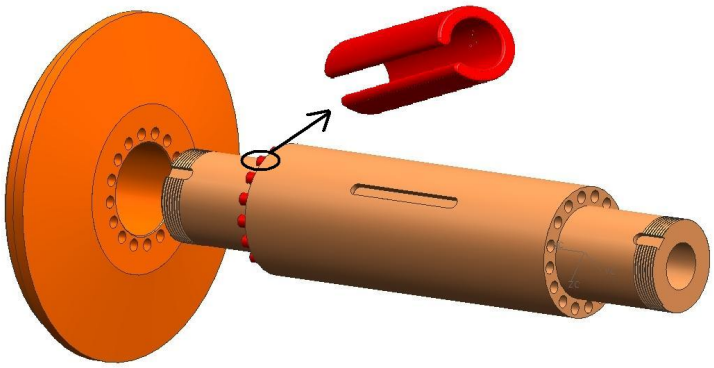

Figure 2.3: The sheave that has to move onto the intermediate shaft with the spring pins

possible a bracket (see figure 2.4) has been made on which all the components of the CVT can be placed (sideways) without the housing. Then one side of the housing can be placed on top of the parts and the entire assembly can be turned over. Finally, the second part of the housing can be placed on its position and the CVT is ready to use.

Figure 2.4: The bracket to assemble the CVT

2.2 Ratio

Compared to a conventional CVT the inline CVT has a very large ratio range in relation to the stroke of the pulley sheave. The ratio of the first CVT is multiplied by the ratio of the second CVT to obtain the overall ratio. The non-linearity of the relation between the stroke $\boldsymbol{\Delta x}$ of the pulley and the ratio slightly decreases, because both CVTs will make a smaller stroke, and therefore operate close to the equilibrium point (ratio=1). If the inline is seen as two CVTs placed in series it is possible to calculate the running radii $\boldsymbol{R_1}$ through $\boldsymbol{R_4}$ and the two individual ratios ($\boldsymbol{r_I}$ and $\boldsymbol{r_{II}}$) as a function of the length of the belt $\boldsymbol{L}$ and the center distance between the pulleys $\boldsymbol{a}$. The general equation for a regular CVT is shown in equation 2.2. Since the strokes of both movable sheaves (equation 2.3) on the idler shaft have to be equal to each other (after all, they are integrated into one movable sheave), it is possible to write for the radius $\boldsymbol{R_{out_I} = R_0 + \Delta R}$ for $\boldsymbol{CVT_I}$ and $\boldsymbol{R_{in_{II}} = R_0 - \Delta R}$ for $\boldsymbol{CVT_{II}}$ where $\boldsymbol{R_0}$ is the radius at ratio= $\boldsymbol{1}$. When this relation is used in equation 2.2 for both the input- and output CVT the different running radii can be calculated. Since this relation cannot be solved algebraically, a program has been written that uses root-finding techniques to solve this problem.

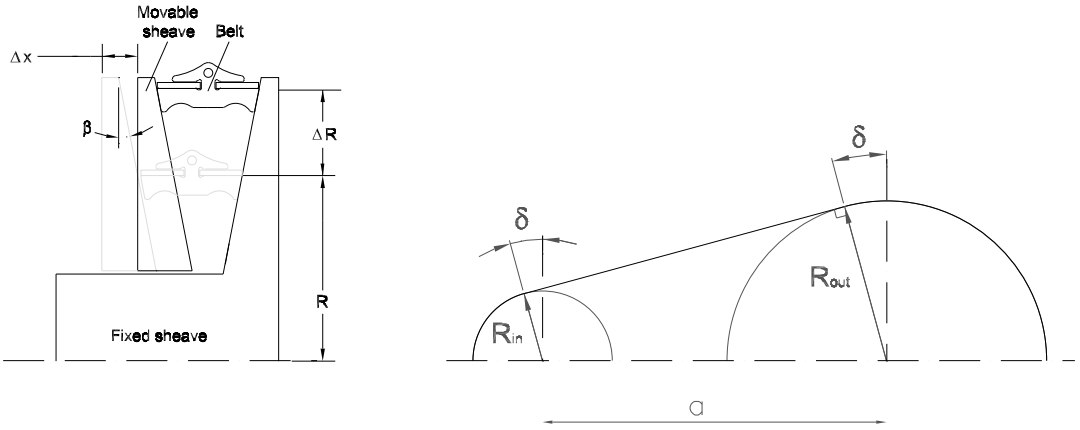

Figure 2.5: Geometry of a pulley

$$\boldsymbol{L} \;=\; \boldsymbol{2\ \arcsin\left(\frac{R_{out}-R_{in}}{a}\right)\ (R_{out}-R_{in}) + \pi\,(R_{out}+R_{in}) + 2a\sqrt{1-\frac{R_{out}-R_{in}}{a^2}}} \tag{2.2}$$

The relation between running radius and stroke is easily given by:

$$\boldsymbol{\Delta x = 2\ \tan(\beta)\ \Delta R} \tag{2.3}$$

The relation between the overall ratio of the CVT and the ratios $\boldsymbol{r_I}$ and $\boldsymbol{r_{II}}$ of the two individual CVTs is shown in figure 2.6. It could be expected that the ratios $\boldsymbol{r_I}$ and $\boldsymbol{r_{II}}$ are the square root of the overall ratio, however, due to the non-linear relation between stroke and ratio, the ratio of $\boldsymbol{CVT_I}$ is always higher compared to the ratio of $\boldsymbol{CVT_{II}}$.

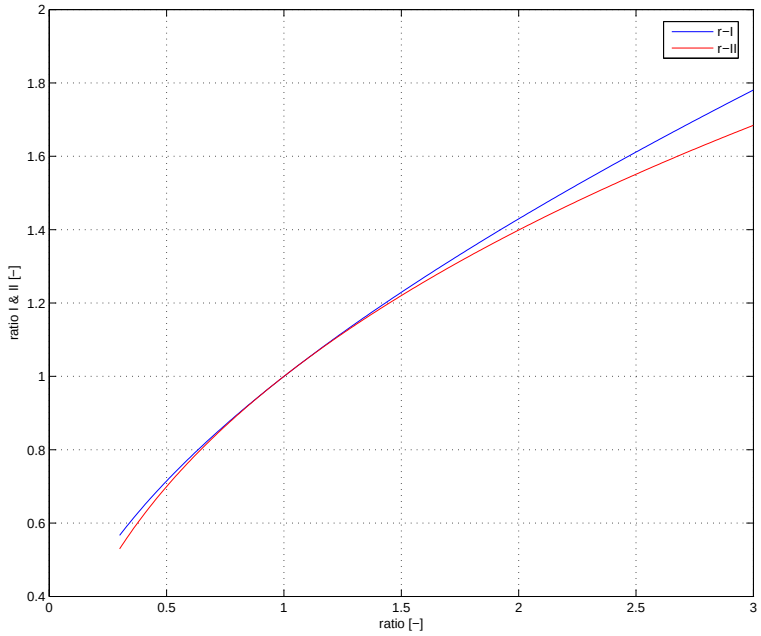

Figure 2.6: $\boldsymbol{r_I}$ and $\boldsymbol{r_{II}}$ as function of the overall ratio

It could be argued that the inline-CVT should not be made symmetrical. The different ratios of the two sets of CVTs as well as the fact that the second CVT has to be able to withstand higher input torques can argue for that. However, since a lot of parts are exactly identical when the CVT is kept symmetrical it is decided not to change that.

2.3 Clamping forces

The relation between overall ratio and the two individual ratios can be used to calculate the running radii of the belt and the torque the second CVT has to transmit. The input and output CVT are now seen as two individual CVTs and the necessary clamping forces for each CVT are calculated using the clamping force theory [vR]. A summery of this theory is shown in appendix A.

The results are shown in figure 2.7. If the chain of the CVT will slip in steady state conditions this will happen on the pulley with the smallest running radius. This pulley is

the critical pulley concerning slip and this is represented in the graphs with a solid line.

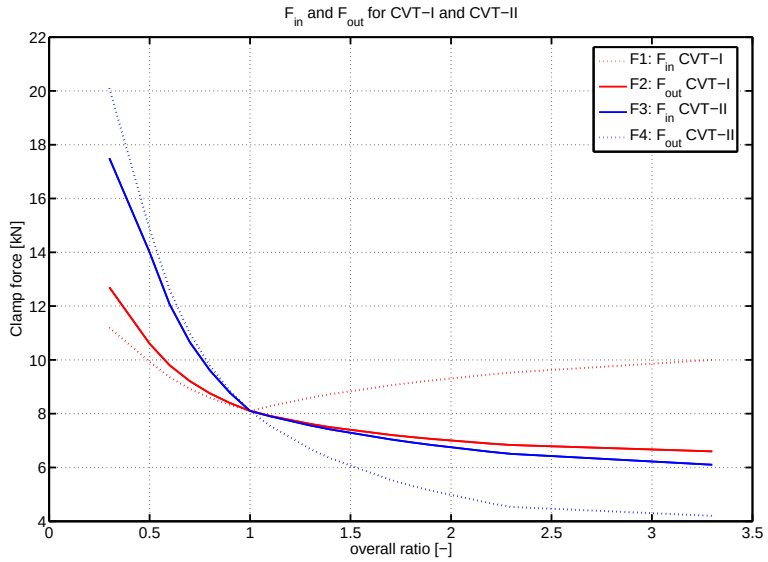

Figure 2.7: $\boldsymbol{F_{in}}$ and $\boldsymbol{F_{out}}$ for $\boldsymbol{CVT_I}$ and $\boldsymbol{CVT_{II}}$ individual

Since the output pulley of $\boldsymbol{CVT_I}$ and the input pulley of $\boldsymbol{CVT_{II}}$ are integrated on one shaft it is not possible to have independent clamping forces, thus $\boldsymbol{F_2 = F_3}$. This means one set of pulleys will always be over clamped completely. This is undesirable for the overall efficiency, however, it is shown in [Sha04] that the efficiency of the GCI-chain is less sensitive to over clamping compared to the Van Doorne belt.

The forces shown in figure 2.7 are calculated for different input torques and to create clamp maps for input and output pulley as shown in figure 2.8. The secondary force will be actively controlled using a servo-hydraulic system. The clamp map will be used as a look up table to create a set point for the required pressure. The primary force is not actively controlled, but corresponds to the pressure that is needed to maintain the ratio. This implementation of this system will be discussed in more detail in chapters 4.

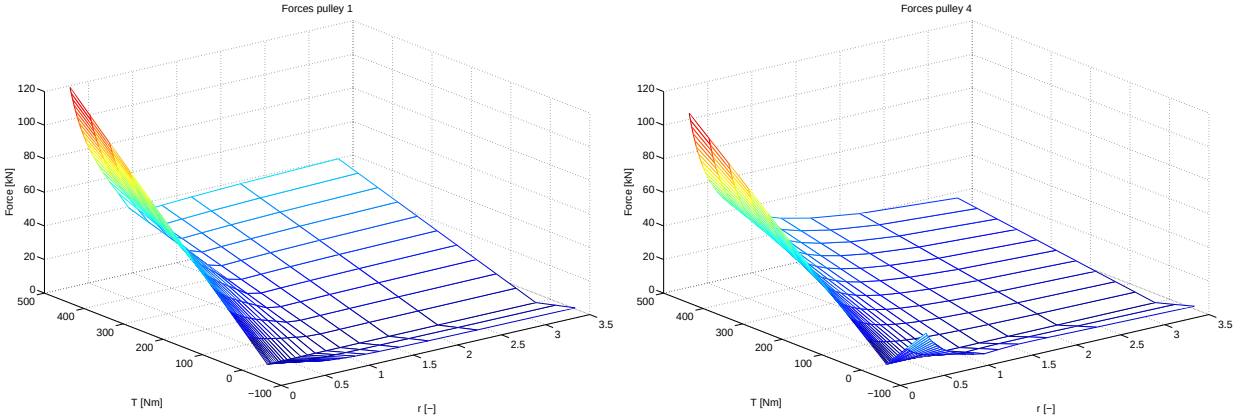

Figure 2.8: Clamp maps for the inline CVT.

2.4 Advantages of the inline CVT

Compared to a regular CVT with the same ratio range the inline CVT has several advantages. First of all, since the ratio of the first CVT is multiplied by the ratio of the second CVT, to achieve the same ratio range as a conventional CVT the two stages of the inline CVT can have a much smaller individual ratio span. Due to this smaller ratio span the CVTs will operate closer around ratio one which will increase the efficiency a bit. Beside that, the radial dimensions of the CVTs can be much smaller since they each only have to cover roughly the square root of the overall ratio. The longitudinal dimension will be slightly increased, but since the inline CVT will be used for rear-wheel driven cars this is no problem. A small disadvantage is the fact that the inline CVT will be slightly larger in vertical direction. Since the type of vehicles in which the CVT will be used have a very large ground clearance this will not be a problem. An other disadvantage of this CVT is that one of the two CVTs will always be over clamped. However, as mentioned, the GCI-chain is not really sensitive for this. Beside that, by using the servo-hydraulic actuation system to power needed to control the CVT will be greatly reduced compared to a conventional system. Due to the symmetrical lay-out of the inline CVT and the relatively small number of parts the costs to produce this CVT compared to an automatic transmission with the same properties will be reduced. Finally, the fact that the input and output shaft lay inline makes it relatively easy to replace the transmission in a rear-wheel driven car by the inline. This makes it possible to sell the CVT as an after-sales device.

Chapter 3

The servo-hydraulic actuation system

To control the CVT in a conventional vehicle there is a fixed displacement oil pump connected to the crankshaft of the engine. A valve is used to control the pressure generated by the pump according to a certain strategy. The lay-out of this conventional system is shown in figure 3.1. The oil pump has to be able to generate enough pressure and flow while the engine runs at its minimum (stationary) speed, which occurs during a take-off of the vehicle, or during an emergency stop. The problem of this system is the fact that the pump will run too fast whenever the engine is not running at its minimum speed. The oil flow becomes too large and a portion of it is bled off by the pressure valve to the sump. This high-pressure flow, which is bled off is a direct loss of energy. Basically, the oil pump uses much more energy than strictly necessary.

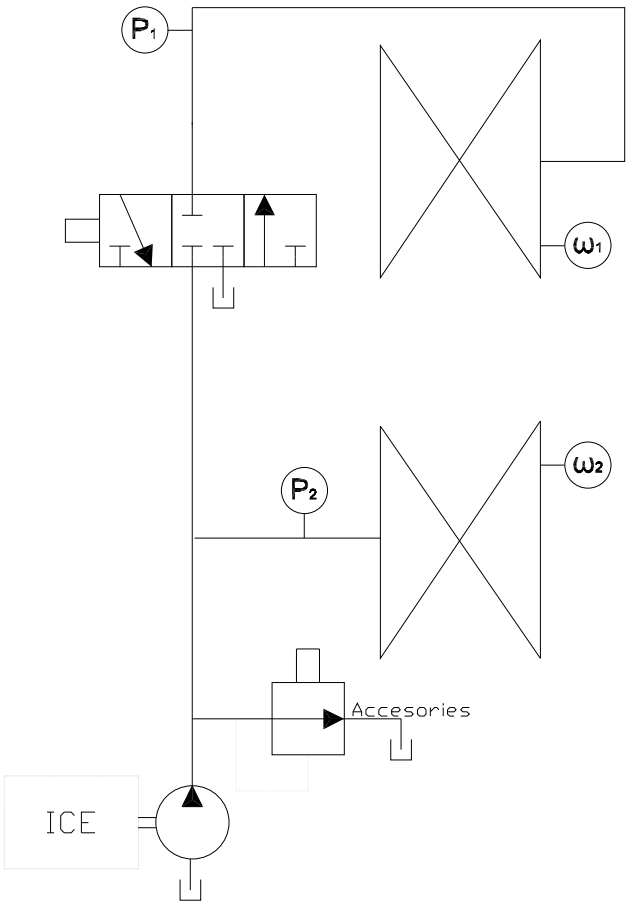

Figure 3.1: The conventional way of CVT control

An alternative way to actuate a CVT is the servo-hydraulic actuation system. The purpose of this system is to reduce the power that is needed to operate a CVT. The idea behind the servo system is to generate the required pressure with the minimal flow possible, hence minimizing the required actuation power.

In this chapter a model for the secondary oil pressure as well as for the energy consumption will be derived. In chapter 4 the influence of different parameters on these models will be discussed according to a real vehicle.

3.1 Servo-hydraulic lay-out

The idea behind the servo-hydraulic actuation system is to use one pump to generate clamping pressure and another pump to change the ratio. These two pumps will be called *clamping pump* and *ratio pump*. In an ideal situation (no leakage) neither pump will rotate

during steady state conditions. However, in reality, both pumps will have to compensate for leakage out of the primary and secondary system. The lay-out of this servo system is shown in figure 3.2 as well as internal leakage of the pump.

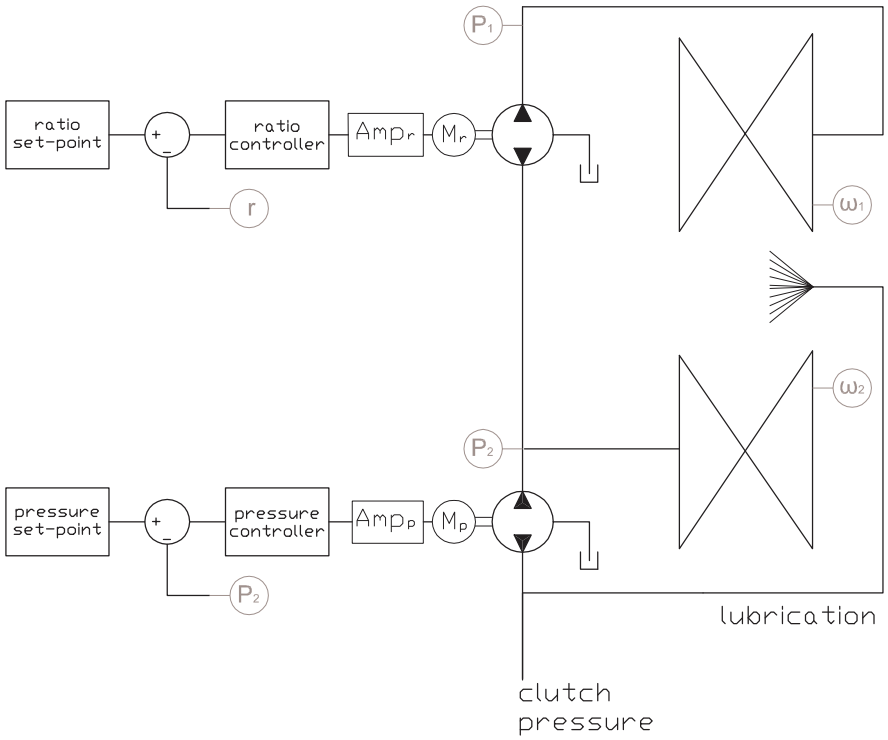

Figure 3.2: The system lay-out of the servo-hydraulic actuation system

When controlling the CVT with the servo system the output of the pressure pump can be connected to the primary or the secondary circuit. Traditionally the secondary pressure is the pressure which is actively controlled while the primary pressure is a result of the required operating conditions of the CVT (mainly ratio and torque). During most operating times the ratio will be larger than one and thus the primary pressure will be larger then the secondary pressure. If it would be decided to control the primary pressure actively this would mean the pressure pump has to generate a certain pressure and the ratio pump has to counter act the pressure already generated by the pressure pump (after all, the secondary pressure is lower). Since the goal is to minimize the control power consumption this is an undesirable situation. Therefore, the secondary pressure is actively controlled with the clamping pump and the primary circuit is connected to the output of the ratio pump.

3.2 Servo amplifier

Both pumps are connected to a servomotor, which is powered by a servo-amplifier. This amplifier transfers a reference signal into three currents going trough the three phases of the servo motor. Most amplifiers can operate in three different modes: current, velocity and position mode. Current-mode means the amplifier has a closed-loop controller which compares the current through the motor with the reference signal. This is the most elementary operation mode. In the velocity mode, an additional speed-loop is placed around the current-loop (see figure 3.3). The speed of the servo-motor is measured and the current is adjusted if the speed is too large or too small. The third mode is the position-mode where the position of the motor can be controlled. This mode is useful if the servomotor is used in a positioning machine, but useless in a CVT. Since none of the three modes can directly control one of the parameters which has to be controlled (clamping pressure or ratio) additional control loops are necessary. Therefore, it is decided to operate both servo-amplifiers in the easiest mode possible, i.e., the current-mode. Using a velocity loop will only result in adding additional dynamics to the system due to the extra controller. These additional dynamics will make it harder to tune the overall control-loop and they will introduce an unknown relation between the required velocity and the actual velocity.

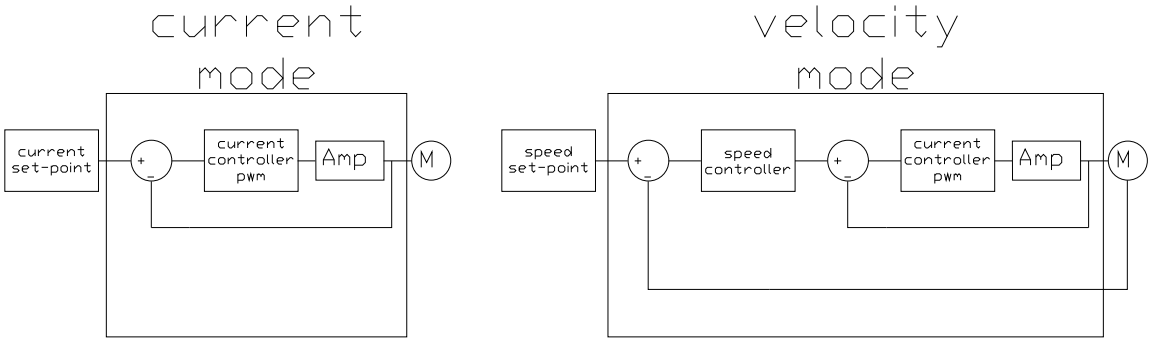

Figure 3.3: Current- and velocity-mode layout of the servo amplifier

3.3 Dynamic model of the oil circuit

Before designing a controller for the pressure and the ratio of a CVT a dynamic model of the secondary oil system is derived which is used for analysis. Different phenomena occur here: electronic, mechanical and hydraulically. The dynamics of the current-controller as well as all other electric phenomena are neglected, since they occur at a frequency which is several magnitudes larger than the dynamics of the CVT. The inertial forces and the friction of the pump and the motor will be taken into account.

Viscous forces, compressibility forces and inertial forces of the oil might have an influence on the system. The relation between those forces is given by two dimensionless numbers:

$$\begin{aligned} \textbf{Cauchy number} &= \frac{\textbf{inertial forces}}{\textbf{compressibility forces}} \\ Ca &= \frac{\rho_{oil}\, v_{oil}^2}{E_b} \\ Ca &= \frac{800\ 2^2}{1e^9} \approx 3.2^{-6} \\ \textbf{Reynolds number} &= \frac{\textbf{inertial forces}}{\textbf{viscous forces}} \\ R_e &= \frac{d\, v_{oil}\, \rho_{oil}}{\mu} \\ R_e &= \frac{8e^{-3}\ 2\,800}{0.1} \approx 128 \end{aligned}$$

Here ρ_{oil} is the density of the oil, v_{oil} is the speed of the oil in the oil channel, E_b is the bulk modulus of the oil, d is the diameter of the oil channel and μ is the dynamic viscosity. The Reynolds number shows that the inertial forces are dominant to the viscous forces. However, the Cauchy number shows the compressibility forces are extremely dominant compared to the inertial forces and thus compared to the viscous forces. If the situation is investigated for the piston in stead of the oil channels these relations will only become more extreme. Therefore, only the compressibility of the oil will be taken into account.

The bulk modulus E_b of the oil is the reciprocal of the compressibility and is given by:

$$E_b = \frac{\dot{p}\, V}{\sum Q} \quad \rightarrow \quad \dot{p_2} = \frac{\sum Q_2\, E_b}{V_2} \tag{3.1}$$

The secondary pressure is given by p_2 and the secondary volume by V_2. When looking at the secondary pressure circuit $\sum Q_2$ can be defined as the sum of the flow generated by the pressure pump Q_p, the flow removed by the ratio pump Q_r and the flow which leaks out of the secondary circuit Q_{l2}.

$$\begin{aligned} \sum Q_2 &= Q_p - Q_r - Q_{l2} \\ Q_p &= \omega_p\, c_p\, \eta_v \\ Q_{l2} &= p_2\, c_{l2} \end{aligned} \tag{3.2}$$

Here c_p is the pump displacement. Note that c_p is often given in $\left[\frac{cc}{rev}\right]$, which equals $\frac{10^{-6}}{2\pi}\left[\frac{m^3}{rad}\right]$. The leakage coefficient c_{l2} relates the leakage to the pressure in the circuit. The leak flow is considered laminar and thus linear with the pressure difference. The volumetric efficiency η_v depends on the rotational speed of the pump and the pressure difference over the pump as is shown in section 4.5 but will be considered constant for simplicity. The part of the leakage that is not constant is partly taken into account in the system leakage.

The flow moved from the secondary to the primary circuit by the ratio pump is Q_r. Under steady-state conditions this flow is equal to the leak flow out of the primary circuit. When this leakage or the ratio of the CVT changes Q_r will change accordingly. At this moment only a steady state situation will be discussed in which the flow is constant and directly linked to the speed of the ratio pump. This speed can be measured and is seen as a (known) error working on the system.

$$Q_r = \omega_r \, c_p \, \eta_v \tag{3.3}$$

The volume of the secondary circuit V_2 depends on the initial volume V_{2_0} and can change due to a changing ratio according to:

$$V_2 = V_{2_0} + \Delta V_2 \tag{3.4}$$

Using equations 2.2 and 2.3 and the area of the piston in the pulley the change of volume ΔV due to ratio change can be calculated. Since this cannot be done algebraically, a look-up table will be used in the simulations. Substituting the different formulas into equation 3.1 gives:

$$\dot{p}_2 = \frac{(\omega_p \, c_p \, \eta_v - \omega_r \, c_p \, \eta_v - p_2 \, c_{l2}) \; E_b}{V_{2_0} + \Delta V_2} \tag{3.5}$$

In equation 3.5, the speed of the ratio- and pressure pump have to be known. Given the fact that the change of ratio ($\dot{r}$) will be much slower than the dynamics of the hydraulic circuit, the ratio can be considered constant when looking at small fluctuations in the pressure. As a result of this, the speed of the ratio pump ω_r will also be constant for small fluctuations in the secondary pressure.

The speed of the pressure pump is not constant. To calculate the acceleration of the pressure pump ($\dot{\omega}_p$) the net torque working on it has to be known. This is the sum of several torques: the torque generated by the motor T_{mp}, the torque generated by the pressure

difference over the pump $\boldsymbol{T_p}$ and static and viscous friction ($\boldsymbol{c_v\ \omega_p}$ and $\boldsymbol{c_s\ sign(\omega_p)}$), where $\boldsymbol{c_v}$ is a viscous friction coefficient and $\boldsymbol{c_s}$ a static friction coefficient. The inertia of the motor plus the pump is given by $\boldsymbol{J_{(m+p)}}$.

$$\dot{\boldsymbol{w}}_{\boldsymbol{p}} \;=\; \frac{\boldsymbol{T_{mp} - T_p - c_v\,\omega_p - c_s\ sign(\omega_p)}}{\boldsymbol{J_{(m+p)}}} \tag{3.6}$$

Using an energy-balance and formula 3.2 for the flow generated by the pump it is possible to calculate the torque $\boldsymbol{T_p}$ generated by the pressure difference $\boldsymbol{\Delta p_p}$. The efficiency of the pump $\boldsymbol{\eta_{pump}}$ is split up into the volumetric efficiency $\boldsymbol{(\eta_v)}$ and mechanical efficiency $\boldsymbol{(\eta_m)}$.

$$\begin{aligned} \boldsymbol{P_{mechanic}\,\eta_{pump}} &= \boldsymbol{P_{hydraulic}} \\ \boldsymbol{T_p\,\omega_p\,\eta_v\,\eta_m} &= \boldsymbol{Q_p\,\Delta p_p} \\ &= \boldsymbol{\omega_p\,c_p\,\eta_v \Delta p_p} \end{aligned}$$

$$\boldsymbol{T_p} \;=\; \frac{\boldsymbol{c_p\,\Delta p_p}}{\boldsymbol{\eta_m}} \tag{3.7}$$

The torque generated by the brushless-DC servo motor is directly related to the current through the motor.

$$\boldsymbol{T_{mp}} \;=\; \boldsymbol{I_p\,K_t} \tag{3.8}$$

The current through the pressure servo motor $\boldsymbol{I_p}$ is the adjustable input of the secondary pressure circuit. The torque sensitivity $\boldsymbol{K_t}$ is a property of the servo motor.

The pressure difference over the pressure pump is equal to the secondary pressure minus the suction pressure $\boldsymbol{\Delta p_p = p_2 - p_{in}}$. The obtained equation for $\boldsymbol{\dot{\omega}_p}$ can be combined with equation 3.5 by differentiating this equation. Now a second order differential equation is obtained for the secondary pressure.

$$\ddot{\boldsymbol{p}}_{\boldsymbol{2}} \;=\; \frac{\boldsymbol{(\dot{\omega}_p\,c_p\,\eta_v - \dot{p}_2\,c_{l2})\ E_b}}{\boldsymbol{V_{2_0} + \Delta V_2}} \rightarrow$$

$$\ddot{\boldsymbol{p}}_{\boldsymbol{2}} + \dot{\boldsymbol{p}}_{\boldsymbol{2}}\left(\frac{\boldsymbol{c_{l2}\,E_b}}{\boldsymbol{V_{2_0} + \Delta V_2}}\right) + \boldsymbol{p_2}\left(\frac{\boldsymbol{c_p^2\,\eta_v\,E_b}}{\boldsymbol{\eta_m\,J_{(m+p)}\ (V_{2_0} + \Delta V_2)}}\right) =$$

$$\boldsymbol{I_p}\left(\frac{\boldsymbol{K_t\,c_p\,\eta_v\,E_b}}{\boldsymbol{J_{(m+p)}\ (V_{2_0} + \Delta V_2)}}\right) + \left(\frac{\boldsymbol{(p_{in}\,c_p - \eta_m\ (c_v\,\omega_p - c_s\ sign(\omega_p)))\,\eta_v\,c_p\,E_b}}{\boldsymbol{\eta_m\,J_{(m+p)}\ (V_{2_0} + \Delta V_2)}}\right)$$

This equation can be written as:

$$\ddot{p} + 2\beta\,\omega_0\,\dot{p} + \omega_0^2\,p = c_1\,I_p + c_2 \tag{3.9}$$

$$\omega_o = \sqrt{\frac{c_p^2\,\eta_v\,E_b}{\eta_m\,J_{(m+p)}\,(V_{2_0} + \Delta V_2)}}$$

$$\beta = \frac{c_{l2}\,E_b}{2\,(V_{2_0} + \Delta V_2)\sqrt{\frac{c_p^2\,\eta_v\,E_b}{\eta_m\,J_{(m+p)}\,(V_{2_0}+\Delta V_2)}}}$$

This is a standard second order system with a natural frequency of ω_0 and a damping coefficient of β. For steady-state conditions $\ddot{p}$ and $\dot{p}$ become zero and the pressure can be written as:

$$p = I_p\left(\frac{c_1}{\omega_0^2}\right) + \left(\frac{c_2}{\omega_0^2}\right) \tag{3.10}$$

$$\left(\frac{c_1}{\omega_0^2}\right) = \frac{K_t\,\eta_m}{c_p}$$

$$\left(\frac{c_2}{\omega_0^2}\right) = p_{in} - \frac{(c_v\,\omega_p + c_s\,sign(\omega_p))\,\eta_m}{c_p}$$

3.4 Centrifugal forces

The forces that clamp the pulleys are not only generated by the two oil pumps but also by the centrifugal effect of the oil in both pulleys. Because of the rotational speed of the pulleys oil is forced to the outside of the pulley and a pressure build up will be the result. The force generated by this has to be taken into account when defining a set point for the pressure pump. In some pulley designs (like the secondary pulley of the Volvo-440) a centrifugal pressure compensation chamber is present, so this effect will not occur. In the inline CVT this centrifugal force has to be taken into account. Generally spoken this centrifugal force depends on the inner and outer diameter of the oil piston (R_{id} and R_{od}) and the density of the oil (ρ_{oil}). If the entry point of the oil channel into the piston is not in the center line of the piston this distance also has to be taken into account, but in the inline CVT this is not the case.

$$F_{cent} = \frac{\pi\,\omega^2\,\rho_{oil}}{4}\left(R_{od}^4 - R_{id}^4\right) \tag{3.11}$$

3.5 Dynamic model of the ratio

As shown in section 3.3 a dynamic model of the oil pressure can be derived. This is useful to analyze the pressure behavior, but not very useful to analyze the dynamics of the ratio of a CVT. Since the bandwidth of the pressure system is expected to be larger compared to the bandwidth of the ratio the dynamics of the oil will be neglected when looking at the ratio. The model of Ide [IUK96] will be used to describe the behavior of the ratio as a function of the force needed to maintain a steady ratio $\boldsymbol{F_1^*}$, the actual force $\boldsymbol{F_1}$ and the speed of the pulley $\boldsymbol{\omega_1}$.

$$\dot{\boldsymbol{r}} \;=\; \boldsymbol{k_r(r)}\;\left(\boldsymbol{F_1} - \boldsymbol{F_1^*}\right)\;|\boldsymbol{\omega_1}|$$

In Ides approach $\boldsymbol{k_r(r)}$ is a value that depends on the ratio and can be experimentally determined. Initially a constant value will be used for simplicity.

3.6 Energy consumption model

Since the main purpose of the servo system is to reduce the amount of power needed to control the CVT the power consumption is examined. Only steady-state conditions are analyzed, since it is very difficult to say anything about dynamic situations. The power consumption under dynamic situations (changing ratio) will depend a lot on how fast this will occur.

Combining equations 3.7 and 3.8 the current in the servomotor can be determined if stated that the load of the pump plus the friction is equal to the torque generated by the motor. This is true when a steady state situation is analyzed.

$$\begin{aligned}
\boldsymbol{T_{m_{[r,p]}}} &= \boldsymbol{T_{p[r,p]} + T_{fric[r,p]}} \\
\boldsymbol{T_{p[r,p]}} &= \frac{\boldsymbol{c_p\,\Delta p_{[r,p]}}}{\boldsymbol{\eta_m}} \\
\boldsymbol{T_{fric[r,p]}} &= \boldsymbol{c_v\,\omega_{[r,p]} + c_s\,sign(\omega_{[r,p]})} \\
\boldsymbol{T_{m_{[r,p]}}} &= \boldsymbol{I_{[r,p]}\,K_t} \\
\\
\boldsymbol{I_{[r,p]}} &= \frac{\boldsymbol{c_p\,\Delta p_{[r,p]}\frac{1}{\eta_m} + c_v\,\omega_{[r,p]} + c_s\,sign(\omega_{[r,p]})}}{\boldsymbol{K_t}}
\end{aligned} \tag{3.12}$$

The servo amplifier chops the voltage to the motor in such a way that the resulting current is equal to the set point. When looking at the RMS value of this current it can be seen as

a continuous signal. If the resistance of the motor is given by $\boldsymbol{R_m}$ and the back-EMF can be described with the voltage constant $\boldsymbol{K_v}$ the electronic power consumption of the pump becomes:

$$\begin{aligned} \boldsymbol{V_{[r,p]}} &= \boldsymbol{I_{[r,p]}}\,\boldsymbol{R_m} + \boldsymbol{\omega_{[r,p]}}\,\boldsymbol{K_v} \\ \boldsymbol{P_{[r,p]}} &= \boldsymbol{V_{[r,p]}}\,\boldsymbol{I_{[r,p]}} = \boldsymbol{I^2_{[r,p]}}\,\boldsymbol{R_m} + \boldsymbol{\omega_{[r,p]}}\,\boldsymbol{K_v}\,\boldsymbol{I_{[r,p]}} \end{aligned} \tag{3.13}$$

In steady-state conditions the pump only has to compensate for the oil leaking out of the system. For the pressure pump, this means it has to compensate for the leakage out of the primary and secondary circuit $\boldsymbol{Q_{l[1+2]}}$ whereas the ratio pump only has to compensate for the leakage out of the primary circuit $\boldsymbol{Q_{l[1]}}$. The speed of the pump $\boldsymbol{\omega_{[r,p]}}$ is given in equation 3.14.

$$\begin{aligned} \boldsymbol{Q_{l[1]}} &= \boldsymbol{p_1}\,\boldsymbol{c_{l1}} \\ \boldsymbol{Q_{l[1+2]}} &= \boldsymbol{p_2}\,\boldsymbol{c_{l2}} + \boldsymbol{p_1}\,\boldsymbol{c_{l1}} \\ \boldsymbol{\omega_p} &= \frac{\boldsymbol{p_2}\,\boldsymbol{c_{l2}} + \boldsymbol{p_1}\,\boldsymbol{c_{l1}}}{\boldsymbol{c_p}\,\boldsymbol{\eta_v}} \\ \boldsymbol{\omega_r} &= \frac{\boldsymbol{p_1}\,\boldsymbol{c_{l1}}}{\boldsymbol{c_p}\,\boldsymbol{\eta_v}} \end{aligned} \tag{3.14}$$

Equations 3.12 and 3.14 can be substituted into equation 3.13 to calculate the power consumption for the pressure and the ratio servo pump. The subscript $\boldsymbol{[r,p]}$ depends on which pump is being investigated. Note that there is a difference between the pressure over one of the two pumps $\boldsymbol{\Delta p}$ and the pressure in a circuit $\boldsymbol{p}$.

Besides this power, the amplifier also dissipates some power to perform its task. This depends on the supply voltage and the current that is generated as shown in figure 3.4. The actual power consumption of a servo-hydraulic actuation system will be discussed in section 4.9.

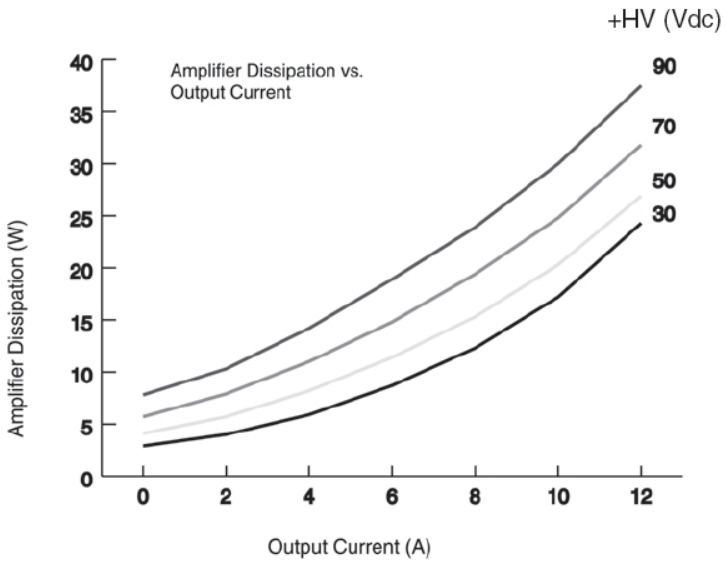

Figure 3.4: Power dissipation of the amplifier

Chapter 4

Implementing the servo-hydraulic system in a vehicle

To be able to test the servo-hydraulic system in a real life situation it is decided to build the system into a stock vehicle. Since the inline-CVT with the hybrid power train was not available anymore an other test platform is chosen. The easiest way to test the system in real life is to build it into a vehicle and to use an older vehicle where there is no electronic communication between the engine management system and the transmission. A Volvo-440 with a VT1-CVT (figure 4.1) from 1996 is chosen for this purpose. The current CVT is fully hydro mechanically controlled and therefore ideal for this purpose.

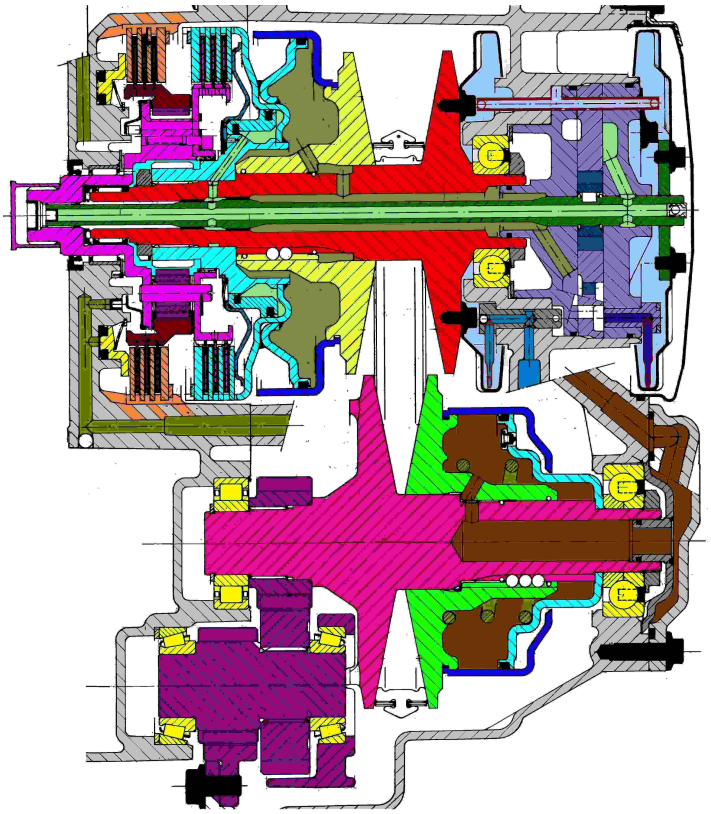

Figure 4.1: The VT1 transmission

All the required hardware (pumps, servo motors, amplifiers, sensors, controller hardware) is chosen based on the specifications which followed from the model derived in chapter 3 and on availability. Specifications of these components are given in appendix C. A datasheet of the used oil can be found in appendix D. The controller will be discussed in more detail in section 4.3.

4.1 Vehicle adjustments: Volvo 440 with VT1-CVT

To be able to control the primary and secondary pressure of the VT1-CVT it is necessary to disconnect the current connections between the hydraulic control unit and both pistons and to connect both pistons to the pressure and the ratio pump. It is relatively easy to connect the secondary piston to the pressure servo pump. There is already a plug available in the housing of the CVT to measure the secondary pressure and this plug will be used to

connect the pump with the piston. Right behind the plug the original oil channel will be blocked to prevent the oil from flowing into the original hydraulic control unit. To connect the primary piston to the ratio pump is a lot more complicated. Due to the lay-out of the housing it is difficult to reach an oil channel, which leads to the piston. It is undesired to use the hydraulic control unit for this purpose, because this unit is still needed to operate the clutches (Drive, Reverse and Neutral) and to regulate the lubrication and cooling flow. Therefore, it is decided to drill a hole through the housing into a small channel, which leads to the primary piston. In this hole a pipe will be pressed and sealed which will be connected to the ratio pump. A spare transmission is used to find out exactly where the hole has to be drilled.

To be able to measure the ratio of the CVT it is necessary to measure the speed of the primary and secondary pulleys. The speed of the primary pulley is measured with a hall-sensor at the primary pitot chamber. Eight small bolts are mounted to this chamber which can be detected by the sensor. The speed of the secondary pulley is measured at the slots for the parking brake. Again, eight slots per revolution are present. In addition to the primary and secondary pulley speed the engine speed is also measured. This is done to detect whether or not the clutch is fully engaged and to determine the engine operating point when the clutch is open.

To determine the input torque of the transmission an engine map is used in combination with the measured engine speed and throttle angle. The throttle angle is measured with a pot-meter. To be able to detect when the brake pedal is touched the voltage of the brake light is measured.

To be able to reach the desired maximum speed the servo-system requires at least a 48 VDC power supply. This is created by placing four small car-batteries in series. A DC-DC converter is used to charge the batteries with the vehicles dynamo. This converter accepts an input voltage somewhere between 7-19 VDC and delivers 55 VDC as output to charge the batteries (4*13.8 V charging voltage). A full electrical scheme is shown in appendix B.

To fit the servo-motors and the pumps under the hood of the car several options have been investigated. The final placement in the vehicle can be seen in appendix E. It is chosen to use pipes to connect all the hydraulic components instead of a hydraulical manifold, because the piping gives a lot more flexibility which is desired due to the lack of space. The DC-DC convertor and the additional batteries are placed directly behind the bumper. The servo amplifiers and the controller are placed in the dashboard because this makes them very accessible.

4.2 Asymmetric pulleys

One of the disadvantages of using a Volvo 440 as test platform is the fact that the primary and secondary pulleys have a different area. This is originally done to make it possible to have a higher clamping force on either the primary or the secondary pulley even though

the primary pressure cannot exceed the secondary pressure. With the servo-system this is undesired. The ratio pump should only shift oil from one circuit to the other. Due to the asymmetric pulleys the clamping pump will have to remove or add additional oil during shifting actions to maintain the same pressure. With a feed forward action in the pressure controller the results from this can be minimized. The energy use is however larger than necessary. In figure 4.2 the total volume of the primary and secondary circuits is shown.

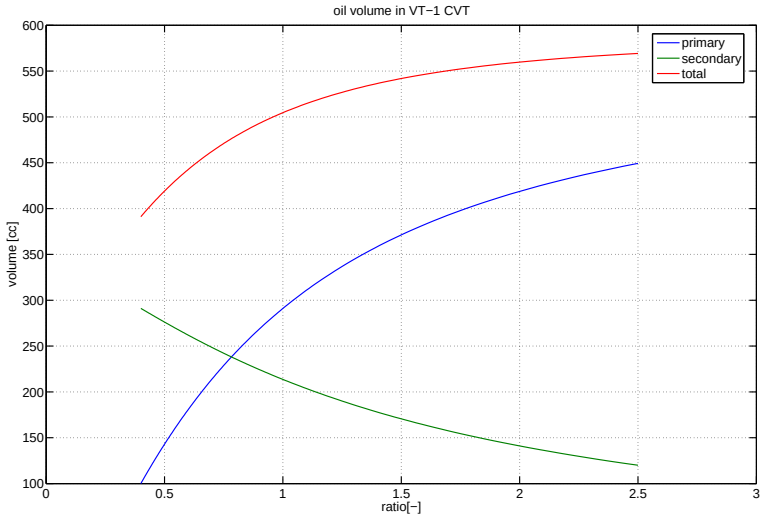

Figure 4.2: Primary, secondary and total oil volume

4.3 Controller hardware

To be able to implement a new actuation system it is necessary to use a physical controller, which can operate as a stand-alone unit. After long elaboration, it was decided to use the UP100 controller from ProDrive Ltd. This is a small, robust unit, which is initially designed for rally-sport purposes. It can be used for many type of control systems found on vehicles and to solve problems faced by engineers developing these control systems [Jam04]. It is used by ProDrive in different demonstrator vehicles, for instance in a hybrid prototype [CJW55]. When using a WindRiver [Win] compiler it is possible to program this controller directly from Matlab/Simulink. In appendix C.1 an extensive list of features of this controller can be found.

Figure 4.3: The UP100 controller from ProDrive

The UP100 controller can operate as a stand-alone unit with its own processor. The maximum operating speed of this processor is $\mathbf{40}\boldsymbol{kHz}$, but it is not possible to run complicated algorithms at this speed. All tested algorithms can easily run at a sample rate of $\mathbf{1}\boldsymbol{kHz}$. It is possible to view the turn-around time, which shows which percentage of a sample is used to calculate the entire control algorithm once. To be able to log data on a PC a serial connection has to be made. It is also possible to log data using the CAN (Control Area Network) connection, but most PCs will not support CAN without additional cards. When logging with the COM-port of a PC the maximum logging rate depends on the number of channels logged and the data resolution used. An optimum between data types (accuracy) and sample rate can be found depending on noise and measurement uncertainties. A problem of logging through a com-port is that it runs under a WindowsXP operating system, which cannot perform real-time tasks. Therefore, the logging of the data is not in real-time. When the computer is busy the sampling rate of the logged data changes.

This results in a measured non-uniform sampling time, even though the controller performs all tasks at a uniform sampling time. In figure 4.4 the sample times of a measured signal are shown.

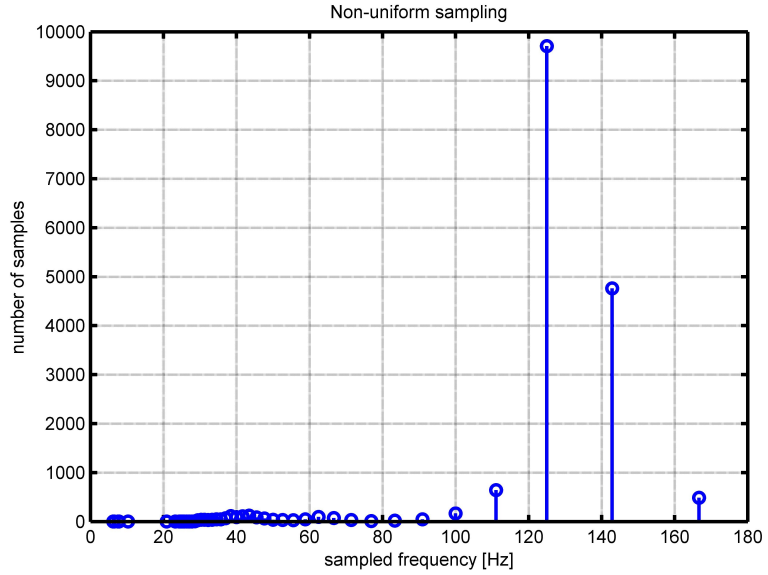

Figure 4.4: The non-uniform sampling times of a measured signal.

In the current configuration there is no data-logging device (flash-card) available on the controller itself. If this card is present, it is possible to record data within the control loop (every time the control algorithm is executed, the requested data can be logged). Then this problem will be solved. Therefore, it is strongly recommended to install the data logger on any controllers bought in the future.

4.4 Set points

To be able to control the CVT it is necessary to generate a set point for the clamping force as well as the ratio. To determine the clamping force the clamping force theory as presented in [vR] is used. A brief summary is given in appendix A. This theory describes the required clamping force depending on ratio, torque and a safety factor. The engine map is used to determine the input torque of the transmission. This algorithm is shown in figure 4.5.

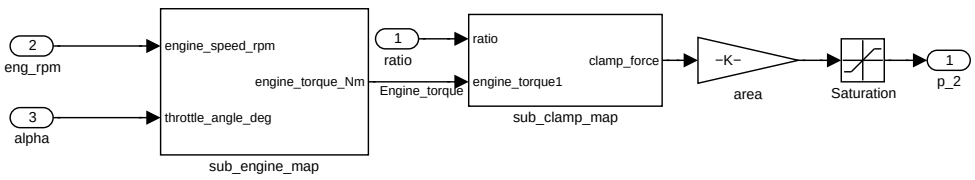

Figure 4.5: The algorithm used to determine the pressure set point

Because the large amount of calculations that have to be done do determine the required clamping force a clamping map is calculated off-line and programmed into the controller as a look-up table. If desired this look-up table can be updated real-time. In figure 4.6 the clamp map, which is currently used can be seen.

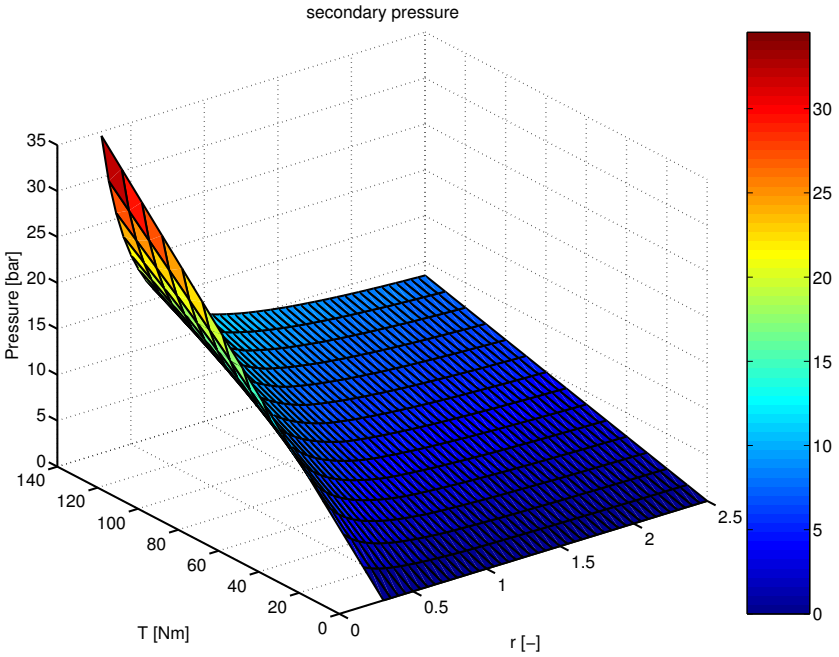

Figure 4.6: The clamp map which is used for set point generation

Unfortunately it is impossible to exactly determine the input torque into the CVT. The usage of a torque-measuring device would be too expensive. However, measurements performed on a this type of engine (1.8L, 1964, B18FP) are available giving information about throttle angle, engine speed, engine torque and fuel consumption. With this information an engine map has been made which is also loaded into the controller. The map is used to determine the torque the engine is generating as a function of throttle angle and engine speed.

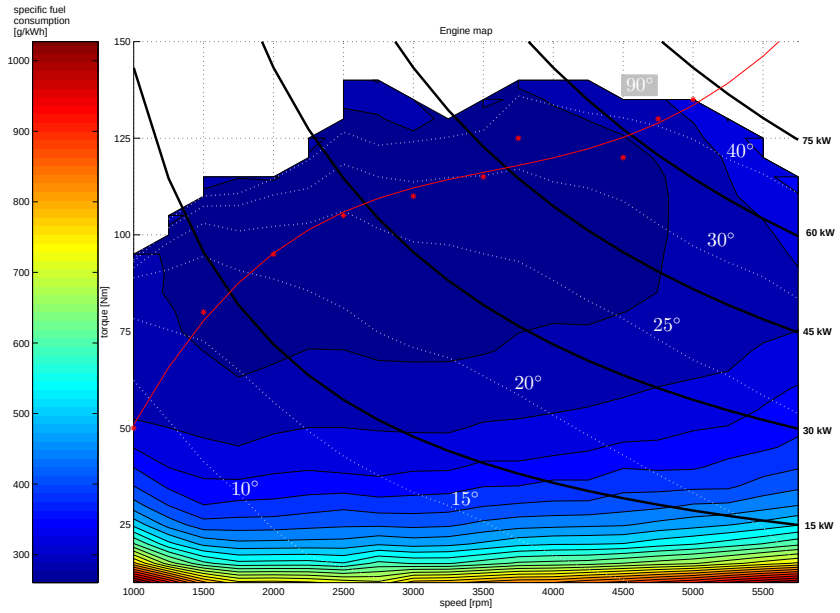

Figure 4.7: The engine map of the Volvo 440 engine with different throttle angles and the IOL.

To create a set point for the ratio the IOL (Ideal Operating Line) can be used. On every line with an equal power output there is a point with the smallest fuel consumption. When all these points are connected the IOL is generated. Sometimes the IOL is also called e-line. It is clear that the points forming the IOL are not on a smooth line. This is due to the limited number of data points available in the engine map as well as the very small fluctuation of the fuel consumption in a rather large area. A smooth line is fitted through the different points to create a workable IOL and a polynomial function is created for this line.

If the engine is always kept on the IOL, there is hardly any torque available to accelerate the vehicle when the pedal is pushed. In section 1.1.1 it was explained how this problem can be solved when using a hybrid power train. Unfortunately, that is not possible with the Volvo 440. The only solution is to operate the vehicle somewhere below the IOL. It is chosen to operate the vehicle at a new line, which is 75% of the IOL. The ratio controller will change the ratio of the CVT in such a way that the engine will operate at this new line. A time delay of 1 second is used to prevent extremely fast shift movements. The ratio set point is limited to prevent the engine running either too fast or too slow. Besides this automatically generated ratio-set point it is also possible to set the ratio by a manual user input. In this way all kind of shifting algorithms can be examined and it can be shown that the controller is able to follow all kind of set points. This project does not focus on designing different shift algorithms.

4.5 Volumetric pump efficiency

In the dynamic model the gear pump is considered to have a constant volumetric and mechanical efficiency. A better approach is to model the pump as an ideal pump in combination with a restricted connection between input and output.

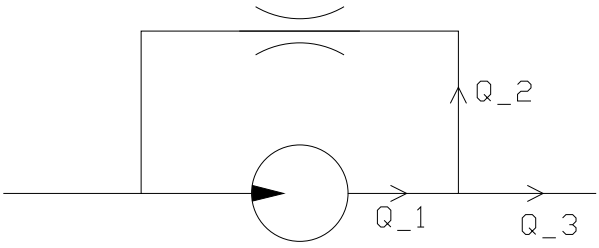

Figure 4.8: The model of the pump

The flow through the gears ($\boldsymbol{Q_1}$) will be linear with the rotational speed $\boldsymbol{\omega}$, and the flow through the restricted connection (the internal 'leakage' $\boldsymbol{Q_2}$) is directly related to the pressure difference ($\boldsymbol{\Delta p}$), the leakage coefficient ($\boldsymbol{c_l}$) and the dynamic viscosity ($\boldsymbol{\mu}$).

$$
\begin{aligned}
\boldsymbol{Q_1} &= \boldsymbol{c_p\,\omega} \\
\boldsymbol{Q_2} &= \boldsymbol{c_l\,\frac{\Delta p}{\mu}} \\
\boldsymbol{Q_3} &= \boldsymbol{Q_1 - Q_2}
\end{aligned}
$$

$$
\begin{aligned}
\boldsymbol{\eta_v} &= \boldsymbol{\frac{Q_3}{Q_1} = 1 - \frac{Q_2}{Q_1}} \\
\boldsymbol{\eta_v} &= \boldsymbol{1 - \frac{c_l}{c_p} \cdot \frac{\Delta p}{\omega \mu}}
\end{aligned}
$$

The factor $\frac{\boldsymbol{c_l}}{\boldsymbol{c_p}}$ is a function of the pump geometry, the clearance and the displacement. This factor is unique for a pump. The other factor, $\frac{\boldsymbol{\Delta p}}{\boldsymbol{\omega \mu}}$ depends on the operating conditions as well as on the medium, which is being pumped.

The efficiency of the pump as a function of operating speed and pressure is shown in figure 4.9. It can be seen that for a higher pump speed the efficiency increases. At very low speeds the internal leakage has a relatively high influence on the net flow. At higher speeds the leakage becomes less significant.

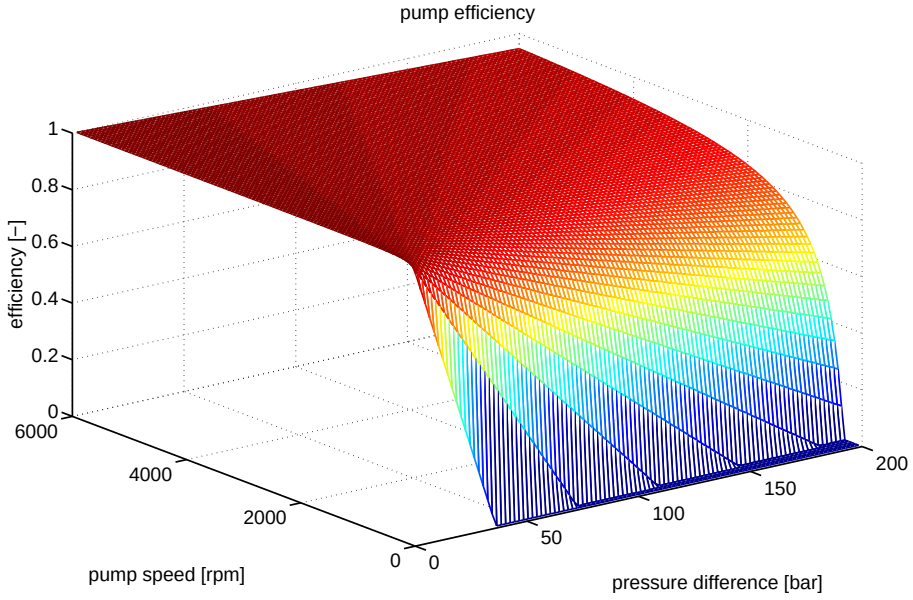

Figure 4.9: The efficiency of the pump at different operating points

Since a large part of the leakage through the pump can also be seen as leakage out of the system this approach will not be used to analyse the dynamic behavior of the oil in the secondary system.

In figure 4.10 measurements on the pump are shown. It can be seen that the mechanical efficiency $\boldsymbol{\eta_m}$ is around 50 %, which is very poor. The static friction coefficient can be determined nd is $\boldsymbol{c_s\ sign(\omega_p) = 0.0154Nm}$. The leakage constant for the secondary circuit can also be determined with this measurement. The very high leakage in the initial measurement was a reason for some concerns. It was expected that there was an unknown leakage somewhere in the transmission as is shown in appendix F. After this leakage has been found and repaired new measurements were done. The leakage constant is expected to be $\boldsymbol{c_{l2} = 1.4e^{-11}}$.

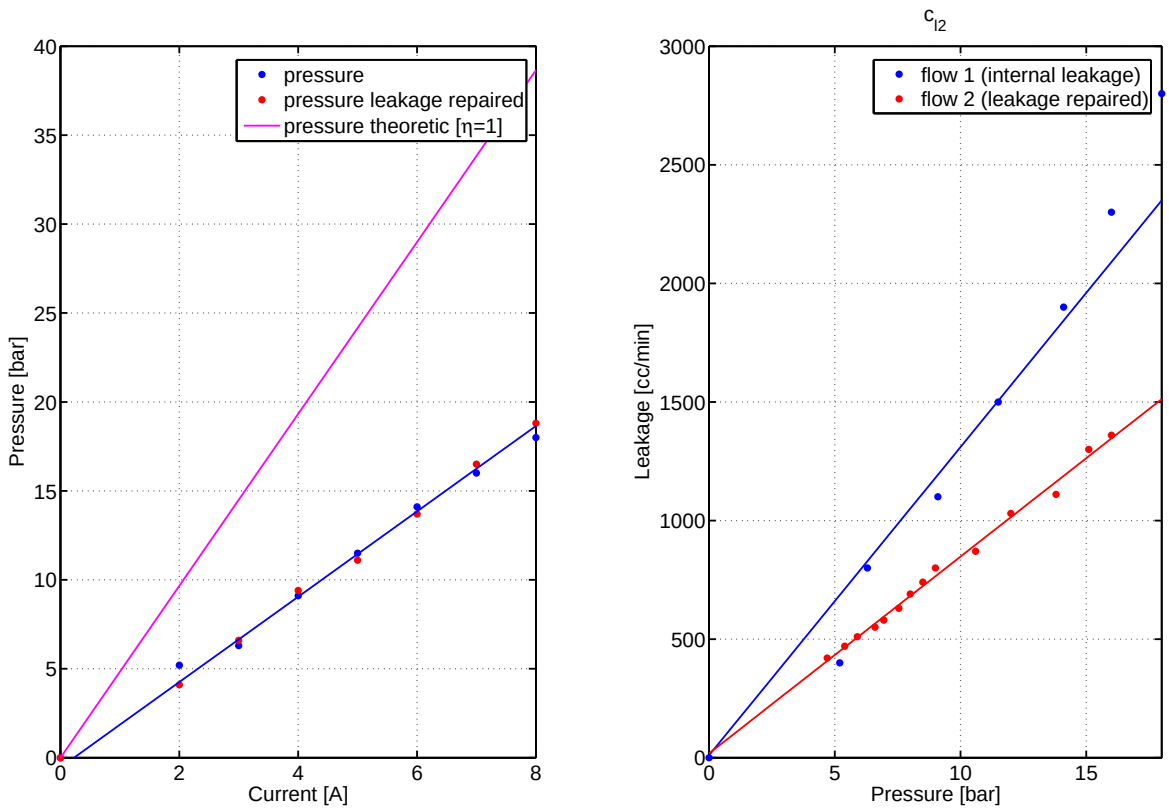

Figure 4.10: The measured characteristics of the pump

4.6 Analyzing the dynamic behavior

A very common technique to determine the transfer function of a system is to measure the frequency response by adding white noise to the output of the controller and to measure the input and the output of the system. When this was tried on the Volvo set-up the correlation between the input and the output was extremely low and the required transfer function was useless. Part of this is caused by an input filter on the servo amplifier (high frequencies are filtered out) and part of it is caused by the fact that the content of the noise signal has to be very small. A stronger noise signal cannot be accepted by the servo amplifier, since the spikes of this signal exceed the maximum input capacity. Therefore, an other approach has to be used to determine the transfer function of the system. Sines with an increasing frequency are send to the amplifier and the set point as well as the resulting pressure are measured. A program has been written which, for every frequency, determines the relation between input- and output amplitude as well as the phase between those two signals. With these points a bode diagram can be plotted.

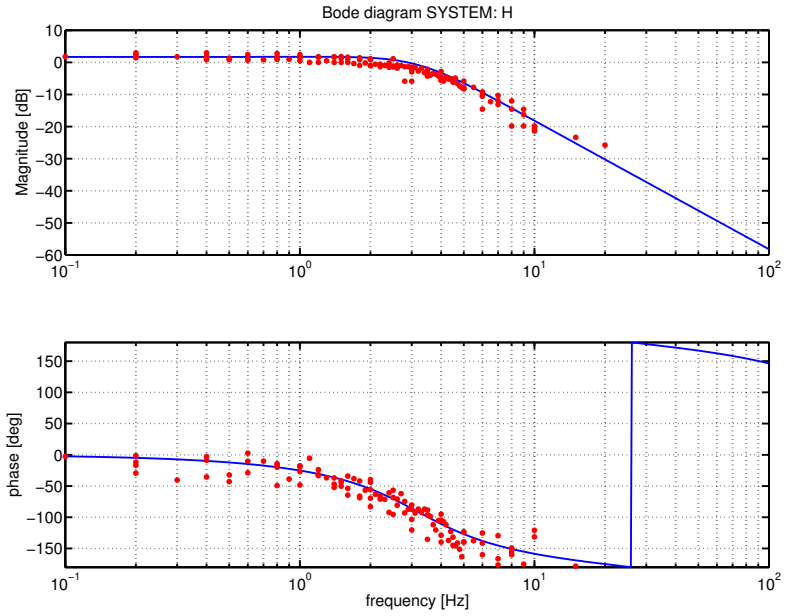

Figure 4.11: The measured and fitted bode diagram of the secondary oil circuit of the VT1 CVT in LOW ratio

Equation 3.9 derived in section 3.3 can be investigated for the parameters of the Volvo. It has to be taken into account that if a continuous system is sampled by a controller (thus in discrete time) additional phase delay will occur. The bode diagram shown in figure 4.11 is based on a continuous time model and the additional time delay. The diagram is used to determine certain parameters. This leads to a natural frequency of the secondary circuit between $\omega_0 = 3Hz$ and $\omega_0 = 4Hz$ and a damping coefficient between $\beta = 0.65$ and $\beta = 0.8$ as a result of the changing volume due to ratio changes. Since the changing dynamics of the system is predictable it makes sense to use gain- scheduling when designing the actual pressure controller.

$$\ddot{p} + 2\beta\,\omega_0\,\dot{p} + \omega_0^2\,p = c_1\,I_p + c_2$$

$$\omega_o = \sqrt{\frac{c_p^2\,\eta_v\,E_b}{\eta_m\,J_{(m+p)}\,(V_{2_0} + \Delta V_2)}}$$

$$\beta = \frac{c_{l2}\,E_b}{2\,(V_{2_0} + \Delta V_2)\sqrt{\frac{c_p^2\,\eta_v\,E_b}{\eta_m\,J_{(m+p)}\,(V_{2_0}+\Delta V_2)}}}$$

To change the damping behavior of the system without changing its natural frequency, the only solution is to adjust the leakage coefficient. This will result in an adjustment

of c_{l2}. The smaller the leakage, the less damped the system will respond. Changing the bulk modulus E_b on purpose is not possible, since this is a material parameter. Due to temperature changes and possibly a changing air-fraction in the oil the bulk modulus might change though. Therefore, it is necessary to be careful not to let any air come into the oil, which can happen at the suction side of the pump when there is not enough oil present. The volume of the secondary circuit can be changed, but this will be very difficult to do on purpose, since this is more or less fixed by the design of the pulleys. However, it can be seen that the pressure circuit will become more damped when ΔV_2 becomes larger (shifting to LOW). This is caused by the oil volume, which acts as a damper. To change the natural frequency of the system it is very effective to change the pump displacement c_p. Again, it is difficult to change the volume or the bulk modulus on purpose. The moment of inertia is also more or less determined by the hardware.

The changing dynamic behavior due to shifting (changing ΔV_2) is shown in figure 4.12. It is not possible to measure the transfer function of the secondary oil circuit when the system is not in LOW. When the transmission is not in LOW the CVT will start to shift as soon as the pressure is changed. A ratio controller is able to keep the ratio constant, but the boundary conditions (primary pressure, leakage) will change due to this. Therefore, the transfer function is only measured in LOW and then calculated for HIGH ratio.

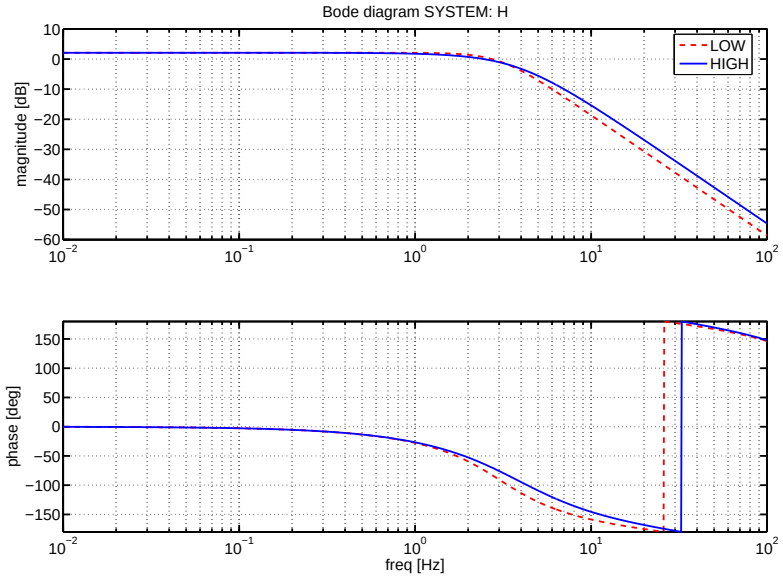

Figure 4.12: The bode diagram of the secondary oil circuit of the VT1 CVT for high and low ratio

Based on the bode diagram shown in figure 4.12 the performance improvement when using gain scheduling (which uses the measured ratio to adjust the different parameters of the controller) for the pressure controller will not be very large, since the dynamic behavior does not change a lot in the different operating points. As mentioned before the VT1-CVT

has a very high leak flow and the efficiency of the pump is very poor. This causes the changing volume to be of less influence on the dynamics of the system. When a bode diagram is plotted for a CVT with less leakage, as shown in figure 4.13, the advantages of a controller with changing parameters will become more significant.

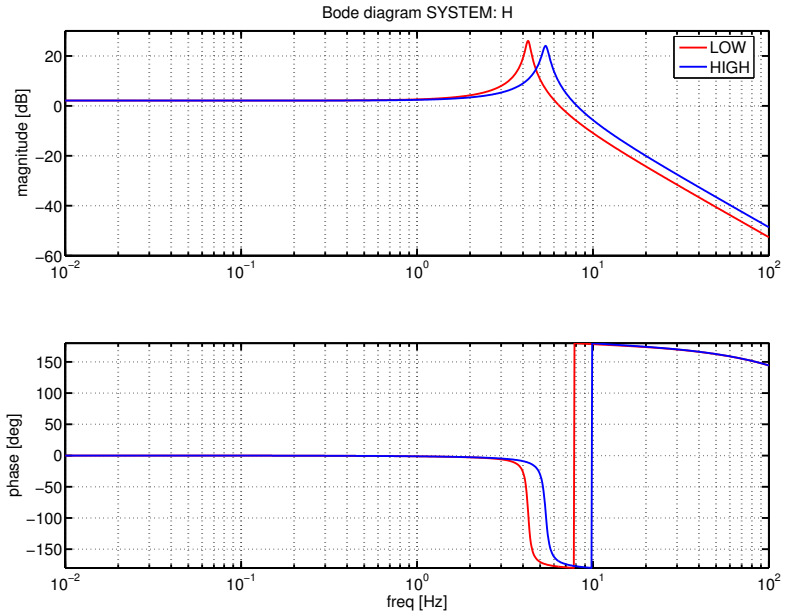

Figure 4.13: A theoretical bode diagram for HIGH and LOW ratio if there would be less leakage.

4.7 Pressure controller tuning

Based on the model of the secondary pressure derived in 3.3 a controller for the clamping pressure can be designed. Loop shaping techniques are used to tune the controller. All differentiator actions are performed by tame differentiators, so measured and discrete signals will not make the controller output grow infinitely. A feed-forward controller is used to compensate for static friction, known inertias and accelerations of the ratio pump.

The theoretical controller consists of a low pass controller to suppress measurement noise, a lead-filter to get some phase lead around the bandwidth and a gain to amplify the set point. Two different controllers are tuned for LOW and for HIGH ratio and a linear interpolation between those points is used for simplicity. Tuning the pressure controller purely theoretically is very difficult, since this depends on many unknown parameters. Therefore, it is chosen to use the controller lay-out and tune the parameters online. To be able to tune the parameters of the pressure controller (secondary pressure) it is decided to temporarily use a pressure loop on both primary and secondary pressure circuit. This

makes it a lot easier to tune the pressure controller, since it is possible to keep the primary pressure constant, but at a different value as the secondary pressure.

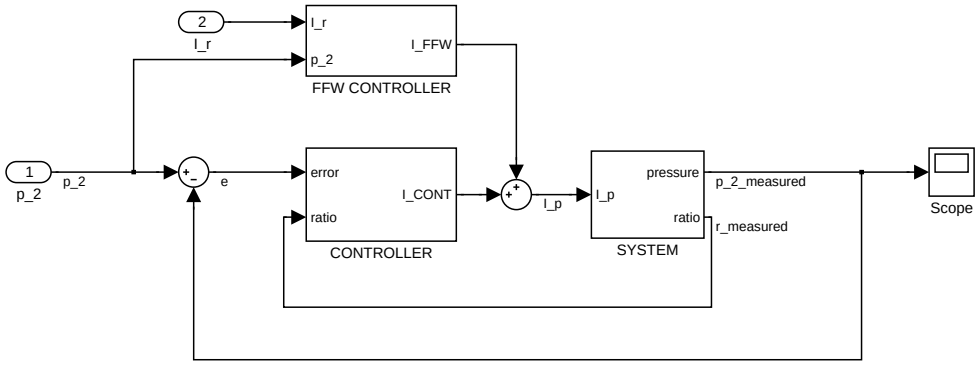

Figure 4.14: The controller lay-out of the pressure controller

$$
\begin{aligned}
C_{low\,pass} &= \frac{1}{\frac{s^2}{(2*\pi*f_{lp})^2} + \frac{1.4s}{2\pi f_{lp}} + 1} \\
C_{lead} &= \frac{\frac{s}{2\pi f_1} + 1}{\frac{s}{2\pi f_2} + 1} \\
C_{gain} &= c \\
C_{total} &= C_{low\,pass}\, C_{lead}\, C_{gain}
\end{aligned}
$$

$$
\begin{aligned}
C_{LOW} &= \frac{0.25s + 10}{1.8e-9s^3 + 3.8e-6s^2 + 3.95e-3s + 1} \\
C_{HIGH} &= \frac{0.19s + 9}{1.54e-9s^3 + 3.34e-6s^2 + 3.54e-3s + 1}
\end{aligned}
$$

With this controller, the secondary pressure circuit is able to reach a theoretical bandwidth of $17.4Hz$, a phase margin of $49°$ at the bandwidth and an amplitude margin of $11.7dB$ in LOW and $20Hz$, $48°$ and $11dB$ in HIGH. In figure 4.15 the bode diagrams of the open-loop system is shown for the LOW ratio for the measured and calculated controller. In appendix H the bode diagrams of the sensitivity, the controller and the closed-loop system are shown as well as the Nyquist-diagram.

If the controller would not use a gain-scheduling algorithm it would be necessary to use the 'HIGH-ratio' pressure controller for the entire ratio range, due to stability issues. This would lead to a decrease in bandwidth from $17.4Hz$ to $12.5Hz$ for the pressure-control loop in LOW ratio. In figure 4.16 the step response of the secondary circuit can be seen.

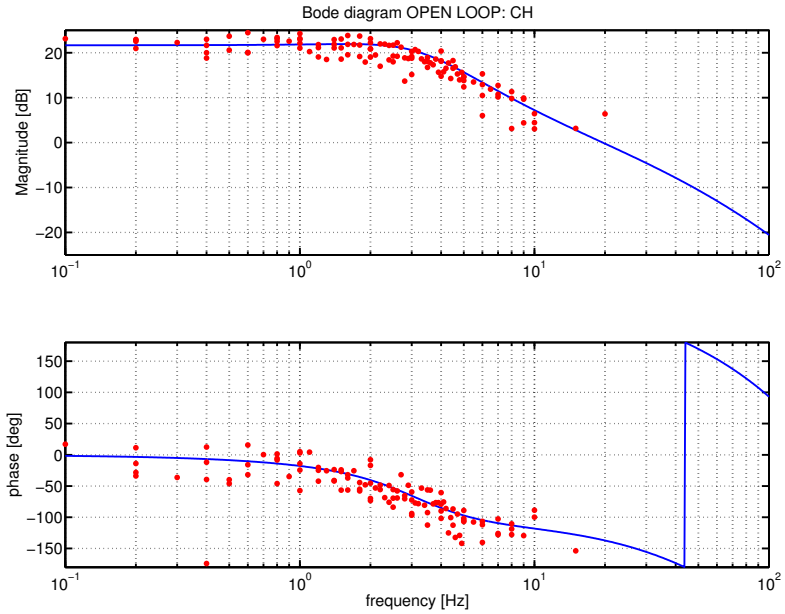

Figure 4.15: The bode diagram of the open loop system

The pressure controller is able to resist disturbances caused by the ratio pump as can be seen in figure 4.17.

During the process of tuning the pressure controller the maximum pressure that could be reached by the system (with and without the controller) dropped a lot. Possible explanations of this will be discussed in appendix G. Because of this pressure limitation, the following measurements are only done for low pressures.

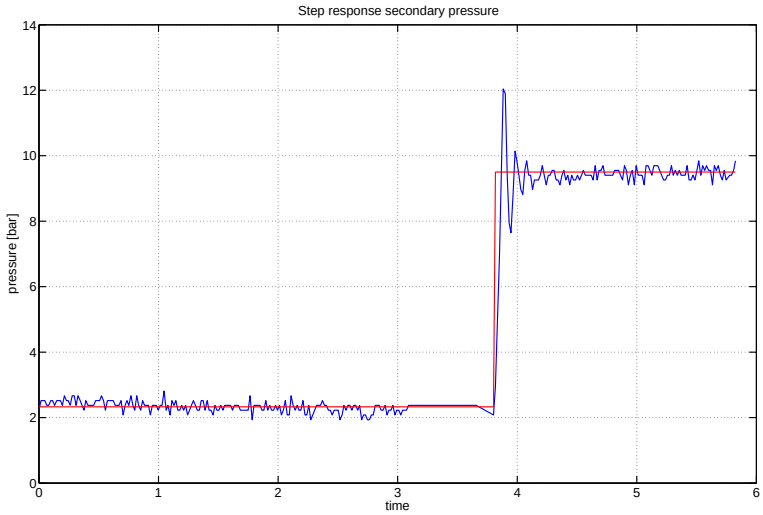

Figure 4.16: step response of the secondary circuit

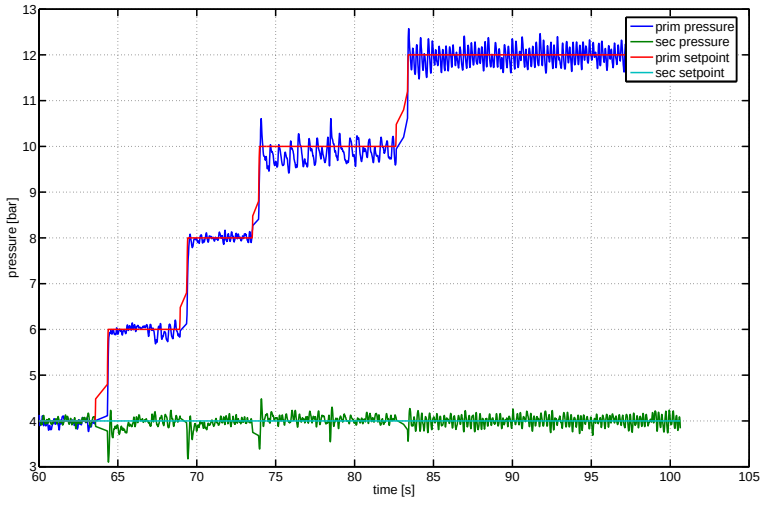

Figure 4.17: Performance of secondary pressure controller with disturbances in primary circuit.

4.8 Ratio controller tuning

The ratio is being controlled with a standard PID-controller which is tuned online on a dynamometer (figure 4.18) of the university.

Figure 4.18: The Volvo 440 at the dynamometer to tune the pressure- and ratio controller.

During larger ratio steps some problems occurred with the secondary pressure. Due to the limitations of the maximum pressure which can be achieved in the secondary system in combination with the poor efficiency of the pump the pressure pump is not able to generate an oil flow, which is high enough to feed the ratio pump and to compensate for the entire leakage. The secondary pressure drops and as a result from the limited flow the primary pressure drops too.

Therefore, the values of the PID-controller had to be lowered to prevent the controller from requiring a too high torque from the ratio pump. Beside this restriction the steps in the ratio-set point had to be limited. If the system is kept within the limitations the ratio controller is able to follow a set point well as can be seen in figure 4.19.

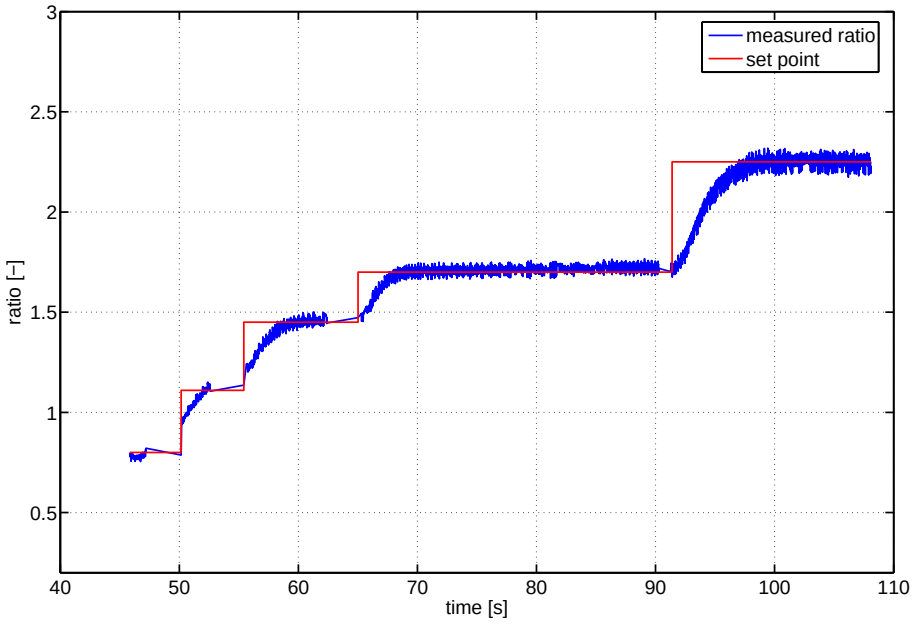

Figure 4.19: Step response of the ratio

It is expected that the ratio pump will be able to shift much faster and accept every possible input if the problems with the pump are solved.

4.9 Power consumption of the servo system

The main purpose of using the servo-system is to reduce the power consumption required to control the CVT. Unfortunately the Volvo set-up is not fully optimized to minimize the control power. The original oil pump is still used to activate the clutches and for lubrication and cooling purposes. The pressure used for lubrication therefore is still higher than required which means unnecessary losses. The leakage in the system is also much too high, when the CVT was designed it was taken into account that there was a very large flow available, so there was no reason to make the seals very accurate. If the CVT would be redesigned this leakage could be reduced thus lowering the power consumption even more. Since it is not possible to optimize this leakage within this project, only the power consumption of the servo system as it is will be discussed without a comparison to the original system. An investigation into all the loss mechanisms for a similar type of transmission is done in [Ake01]. In section 3.6 equations 3.12, 3.13 and 3.14 are derived describing the power consumption of the servo hydraulic actuation system.

$$\boldsymbol{P_{[r,p]}} \;=\; \boldsymbol{I^2_{[r,p]}}\,\boldsymbol{R_m} + \boldsymbol{\omega_{[r,p]}}\,\boldsymbol{K_v}\,\boldsymbol{I_{[r,p]}}$$

$$
\begin{aligned}
I_{[r,p]} &= \frac{c_p\,\Delta p_{[r,p]}\frac{1}{\eta_m} + c_v\,\omega_{[r,p]} + c_s\,sign(\omega_{[r,p]})}{K_t} \\
\omega_p &= \frac{p_2\,c_{l2} + p_1\,c_{l1}}{c_p\,\eta_v} \\
\omega_r &= \frac{p_1\,c_{l1}}{c_p\,\eta_v}
\end{aligned}
$$

In figure 4.20 the power consumption of both servo motors is shown for steady state conditions. In appendix G, the power consumption of both servo motors individually is shown.

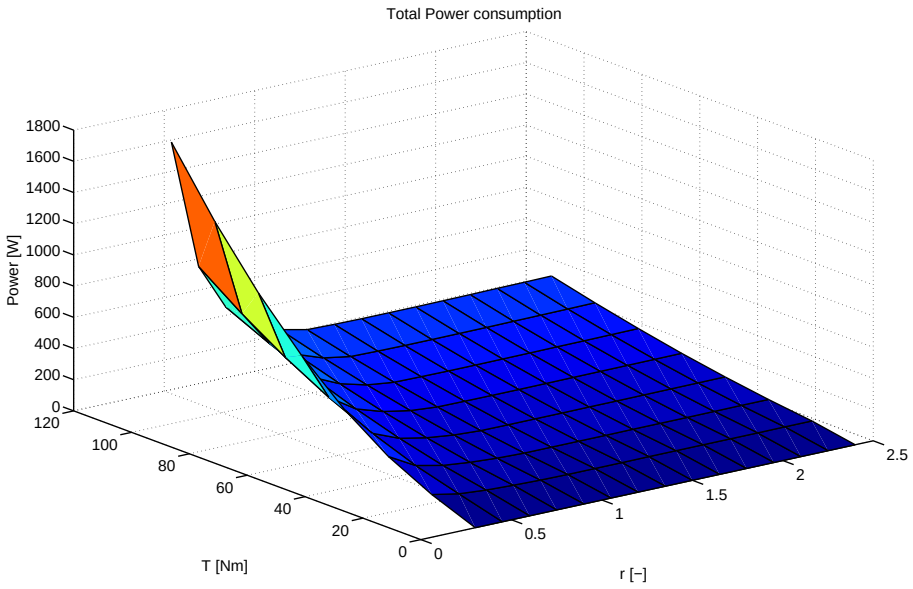

Figure 4.20: The power consumption of the servo system in the Volvo VT1.

The pressure servo motor consumes most of the energy. When driving in a low ratio and at very high input torques, the system consumes almost $\mathbf{2kW}$ of energy. However, this point is only used when taking off with the vehicle. Under normal driving conditions this system will not consume more then $\mathbf{600W}$. This is still a lot, mainly due to the high leakage. There are several ways to improve the power consumption of the servo system. If the leakage would be reduced to a value of $\mathbf{250cc/min}$ at a pressure of $\mathbf{35bar}$ (take-off point, $\boldsymbol{c_{l2} = 1.19e-12}$) and the friction in the pump would be reduced, the peak power consumption ($\mathbf{@150Nm}$ and low ratio) will already drop from almost $\mathbf{2kW}$ to $\mathbf{200W}$. In figures 4.21 and 4.22 the theoretical power consumption with the reduced leakage and friction is shown.

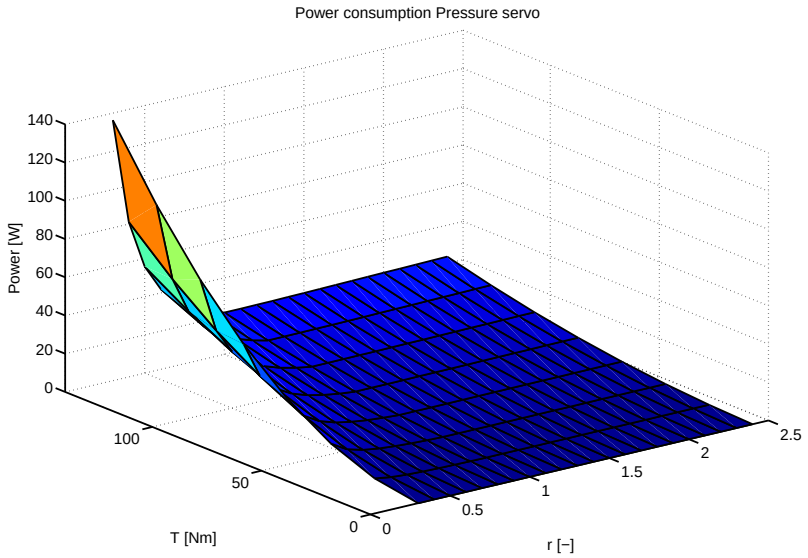

Figure 4.21: The theoretical power consumption of the pressure-servo motor.

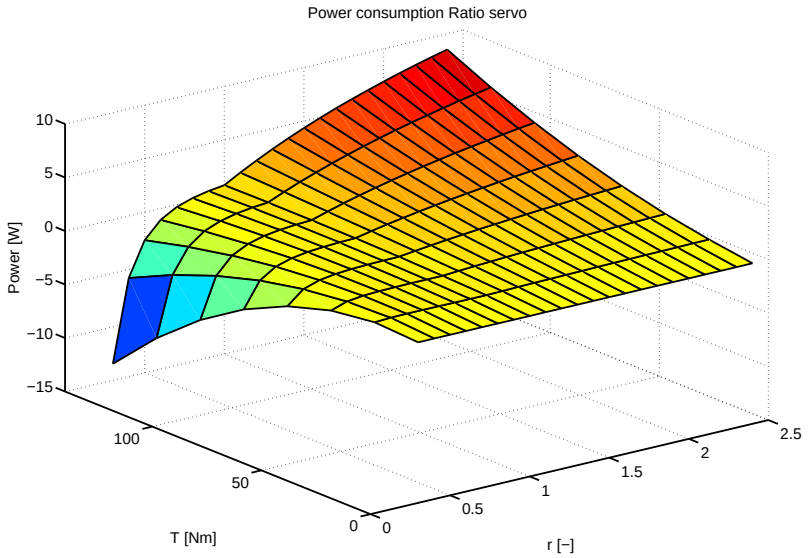

Figure 4.22: The theoretical power consumption of the ratio-servo motor.

It stands out that the ratio pump generates energy when taking of with the vehicle. The oil flow through this pump is in positive direction (from the secondary circuit into the primary), but the torque is in negative direction since the secondary pressure is larger then the primary pressure. This is caused by the different piston areas in this CVT. In a CVT where both pistons have an equal area, this phenomenon will not occur.

Besides limiting the leakage and friction, there are other ways to influence the power consumption of the servo system. The area of the pistons could be enlarged which would require the pressure to create an equal force to become smaller. This will result in a lower torque required to create that pressure and thus a lower current. However, the pump will have to run faster to produce the same flow. It can be seen from equation 3.13 and equation 3.12 that the power consumption will become less when the area is increased. Reducing the pump displacement $\boldsymbol{c_p}$ will also reduce the power consumption. The second term of equation 3.13 will remain the same ($\boldsymbol{\omega\, c_p}$ remains the same) but the first term will decrease. Finally the motor constant $\boldsymbol{K_t}$ could be increased. The same current would then produce a higher torque. Due to the design of the motor, this is very difficult.

It has to be taken into account when optimizing the power consumption of the servo system that all suggestions to decrease the consumption require a lower torque/current but a higher motor speed. In dynamic situations (shifting) the maximum motor speed becomes of importance, since it is necessary to pump a certain volume of oil in a limited time. How long this can be (how long can it take to shift) is open to debate.

If a CVT is required to shift in 2 seconds through the entire ratio range, the power consumed by both servo motors will be roughly the same. Using two identical motors requires a ratio pump to have twice the displacement of the pressure pump to generate enough flow. Of course these assumptions depend a lot on the friction and the leakage and the shifting requirements of the system.

Due to the pressure limitations, which occurred during the course of measurements (see appendix G), it was not possible to measure the power consumption for the entire ratio and torque span. To be able to compare the theoretically required power consumption with some measurements, the power consumption from the pressure pump has been calculated for different values for primary and secondary pressures. For these measurements, all coefficients are determined again based on the new situation. It is shown in figure 4.23 that the model and the measurements are very similar. Based on these measurements it is expected that the true power consumption of the servo system will be the same as the calculated values discussed earlier.

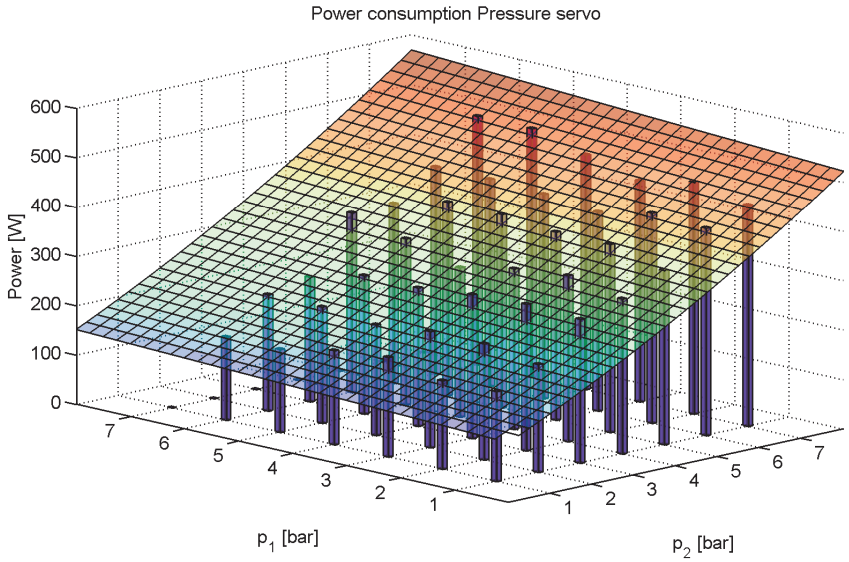

Figure 4.23: The measured and calculated power consumption of the pressure servo motor.

Chapter 5

Conclusions and recommendations

5.1 Conclusions

This Masters thesis is part of a project to build a hybrid vehicle with a CVT. It is explained why a parallel, battery dominant, plug-in hybrid is the preferred configuration for this vehicle. Such a hybrid power train has many degrees of freedom and therefore it requires a sophisticated power train controller. A fundamental power train controller, which takes all boundary conditions into account is designed and can be used to optimize the performance of the hybrid vehicle concerning fuel consumption, emissions or performance.

Since there is currently no CVT available which could be used in the existing hybrid a new type of CVT, called the inline-CVT, has been designed by UC-Davis. The concept of this CVT has been proven by realizing a prototype, and the typical behavior of this transmission has been discussed. To gain more insight in the performance of the inline-CVT the transmission should be installed in a test rig to perform loaded tests. This is partly done by Guus Arts and Niels Scheffer who visited Davis after me. When these tests are completed the CVT should be built into the vehicle.

The inline-CVT is actuated by a servo-hydraulic system. This system has been modeled to analyse the dynamic behavior and this model is used to tune the low-level CVT controller. It is shown that the model describes the behavior of the system well. The model is also used to calculate the power consumption. The expected and measured power consumption are very similar.

To gain experience with the servo system it is built into a vehicle. The original transmission has been adjusted where necessary, all components are bought and the servo system was built into the vehicle and tested. Initially it performed well, but during the tests something happened, which caused the performance of the system to collapse. Due to time limitations it is not feasible to fully investigate the cause of this, but possible causes are discussed.

5.2 Recommendations

The power train controller that has been designed should be optimized to minimize fuel consumption and emissions of the vehicle. To be able to do this it is necessary to have more information about the inline-CVT concerning efficiency and shifting behavior. Therefore, it is required to place this transmission on a test rig to perform a wide range of tests. This is currently being done at UC-Davis.

The goal of the servo-hydraulic actuation system is to minimize the power consumption to actuate a CVT. Therefore, the internal leakage of the CVT should be as small as possible. When an existing CVT is used, the leakage should be reduced if possible. The two pumps which are used for the servo system are quite rare in the conventional hydraulic world. Most gear pumps are designed for much higher pressures than required, thus introducing a relatively high friction. Pumps with a high efficiency and low friction should be used.

In the Volvo set-up the pressure pump caused a problem. The problem with the friction and the efficiency, which showed up during testing should be solved before this project is continued.

Based on the characteristics of the servo system it is recommended to use two identical motors, but two pumps with a different displacement. A ratio pump with twice the displacement of the pressure pump is capable of shifting faster while the pressure difference which this pump has to overcome is smaller.

While implementing the servo system into the Volvo some practical issues occurred. The controller hardware that was finally chosen does not have the possibility to log data in real-time, but logs data on a PC by means of a com-port. This causes the measured signal to have a non-uniform sample time. Therefore, it is not possible to use certain techniques to analyse the system, because they require a uniform sampling time. It is recommended to carry out the controller with an on-board flash card, which can log data in real time. This will simplify the analysis substantially.

To measure the throttle angle a linear potentiometer is used. Due to the shape of an engine map it might be worth to use a logarithmic potentiometer. Initially a slight increase of the throttle angle will result in a large increase of the available torque while near the maximum throttle angle there is only a small increase of available torque when the pedal is pushed further.

When the presented recommendations are taken into account the servo-hydraulic actuation system turns out to be a suitable system to actuate a CVT.

Appendix A

Clamping forces

The clamping force theory is elaborately explained in [vR]. A brief summary will be given here.

In order to calculate clamping forces, it is necessary to understand the torque transmission mechanism in a CVT. Figure A.1 shows the force distribution in a v-belt drive CVT. The vectors drawn perpendicular to the chain represent the magnitude of the tension force acting on the chain at a particular point. A positive torque input is shown For the case shown the torque input is positive, which means that the torque is applied in the direction of rotation. This also results in F1 being greater than F2.

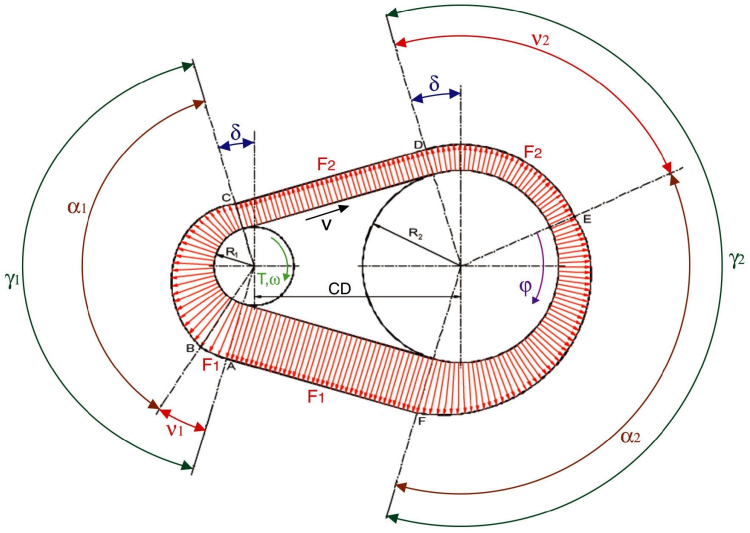

Figure A.1: Angles used in the Clamping Force theory

The contacting arcs $\boldsymbol{\gamma_1}$ and $\boldsymbol{\gamma_2}$ depend on the geometric ratio $\boldsymbol{r}$ and are given by the following equations:

$$\begin{aligned} \gamma_1 &= \pi - 2\,\delta \\ \gamma_2 &= \pi + 2\,delta \\ \gamma_2 - \gamma_1 &= 4\,\delta \end{aligned}$$

Six different regions can be distinguished along the chain, starting from the primary pulley chain entrance:

- From point A to point B: angle 1 is the primary pulley rest arc, the tension force is constant and equal to F_1.
- From point B to point C: angle α_1 is the primary pulley active arc, the tension force decreases gradually from F_1 to F_2.
- From point C to point D: slack side of the chain, the force is constant and equal to F_2.
- From point D to point E: angle ν_2 is the secondary pulley rest arc, the tension force is constant and equal to F_2.
- From point E to point F: angle α_2 is the primary pulley active arc, the tension force increases gradually from F_2 to F_1.
- From point F to point A: tight side of the chain, the force is constant and equal to F_1.

The formula of Eytelwein describes the force distribution in a v-groove belt system:

$$F(\varphi) = F_2\, e^{\frac{\mu\varphi}{\sin\beta}} \qquad (0 \le \varphi \le \alpha) \tag{A.1}$$

Here β is the angle of the sheave ($11°$) and μ is the friction coefficient.

Now it can be shown that for positive torques the clamping forces can be described with the following equations.

$$F_1 = \left(\frac{\cos\beta}{2\mu} + \frac{e^{\frac{\mu\alpha_s}{\sin\beta}}}{e^{\frac{\mu\alpha_s}{\sin\beta}} - 1} \cdot \frac{\gamma_1 - \alpha_s}{2\tan\beta}\right) \cdot \frac{T}{R_1} \tag{A.2}$$

$$F_2 = \left(\frac{\cos\beta}{2\mu} + \frac{1}{e^{\frac{\mu\alpha}{\sin\beta}} - 1} \cdot \frac{\gamma_2 - \alpha}{2\tan\beta}\right) \cdot \frac{T}{R_1} \tag{A.3}$$

For negative torques the angles shown in figure A.1 change. The clamping forces then are described by other equations.

$$\boldsymbol{F_1} = \left(\frac{\cos \boldsymbol{\beta}}{\boldsymbol{2\mu}} + \frac{\boldsymbol{1}}{\boldsymbol{e^{\frac{\mu \alpha_s}{\sin \beta}} - 1}} \cdot \frac{\boldsymbol{\gamma_1 - \alpha_s}}{\boldsymbol{2 \tan \beta}} \right) \cdot \frac{\boldsymbol{T}}{\boldsymbol{R_1}} \tag{A.4}$$

$$\boldsymbol{F_2} = \left(\frac{\cos \boldsymbol{\beta}}{\boldsymbol{2\mu}} + \frac{\boldsymbol{e^{\frac{\mu \alpha_s}{\sin \beta}}}}{\boldsymbol{e^{\frac{\mu \alpha}{\sin \beta}} - 1}} \cdot \frac{\boldsymbol{\gamma_2 - \alpha}}{\boldsymbol{2 \tan \beta}} \right) \cdot \frac{\boldsymbol{T}}{\boldsymbol{R_1}} \tag{A.5}$$

A comparison between this clamping force theory and the VDT-model is done in [Nel03]. It is shown that the maximum difference in calculated clamping force is 15 % higher with the VDT model and this difference occurs at low ratio.

Appendix B

Electrical schemes

B.1 Amplifier connections

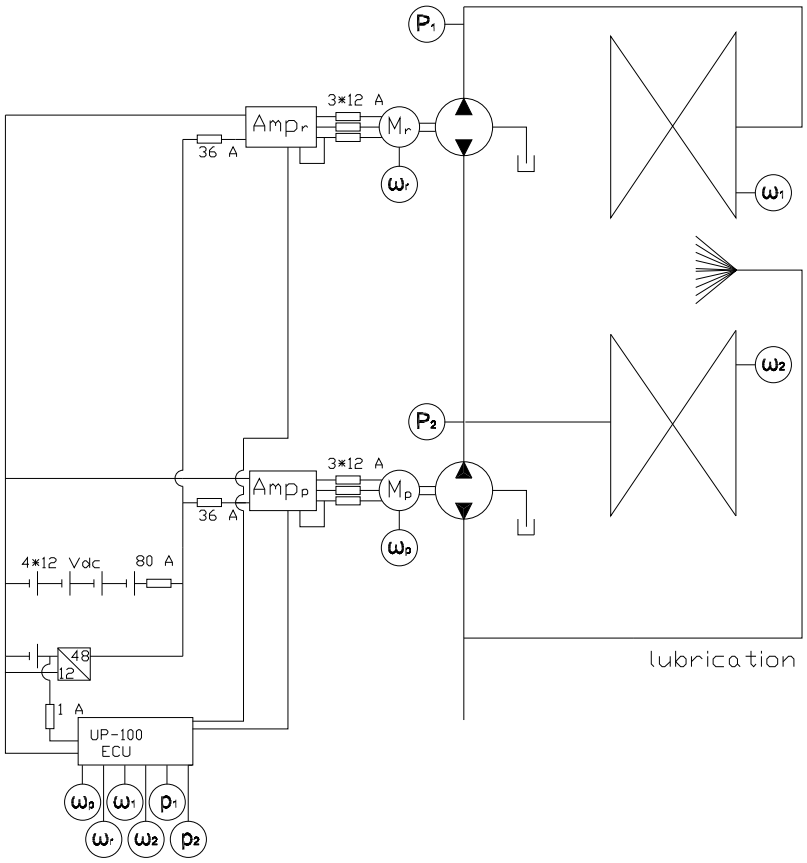

Figure B.1: Schematic system lay-out

B.2 Controller wiring

UP100 pin	Description	CPU-pin	Signal	Wire color
1	Battery positive			Brown
2	Digital Output 7	TPUA14		
3	RS232 Rx - 1	RXD2		
4	RS232 Tx - 1	TXD2		
5	RS232 Rx - 2	RXD1		
6	RS232 Tx - 2	TXD1		
7	Digital Output 1	TPUA8	PWM REF P	Yellow
8	Digital Output 2	TPUA9	Dir P	Green
9	Digital Output 3	TPUA10	PWM REF R	Yellow
10	Digital Output 4	TPUA11	Dir R	Green
11	Analogue Output 1	MPWM0		
12	Analogue Output 2	MPWM1		
13	Digital Output return			
14	Digital Input Ground			
15	Digital Input 0	TPUA0	ω_p	Brown
16	Digital input 1	TPUA1	ω_r	Brown
17	Digital input 2	TPUA2	Brake	White/Black
18	Digital input 3	TPUA3	ω_{ice}	White
19	Digital input 4	TPUA4	ω_1	White
20	Digital input 5	TPUA5	ω_2	White
21	Analogue Input 0	QADCA0	Fault - P	Pink
22	Analogue input 1	QADCA1		
23	Analogue input 2	QADCA2	Fault - R	Pink
24	Analogue input 3	QADCA3		
25	Analogue input 4	QADCA48		
26	Analogue input 5	QADCA49		
27	Analogue input 6	QADCA50	p_1	White
28	Analogue input 7	QADCA51		
29	Analogue input 8	QADCA52	p_2	White
30	Analogue input 9	QADCA53	α	White
31	Digital Output 5	TPUA12		
32	Digital Output 6	TPUA13		
33	5 V sensor supply			
34	12 V sensor supply			
35	Analogue ground			
36	Ditigal Output 8	TPUA15		
37	Battery Negative			

The pins on the UP100 have a different pin-number as on the processor. The table shows the pins on the UP100, their function, the corresponding pin number on the CPU, the function

for which it is used and the color of the wire which is connected. The two accelerometers and the temperature sensor of the CPU are only available on the CPU itself. They are not connected to any of the pins of the UP100.

Description	CPU-pin
Accelerometer X	QADCA55
Accelerometer Y	QADCA56
ECU temp sensor	QADCA57

Appendix C

Hardware specifications

C.1 Prodrive UP100 controller

In this appendix detailed specifications of the UP100 controller will be given [Pro03] and some practical issues will be discussed.

Overview

μProteus is a highly compact and rugged electronic control unit. Despite its size the unit is capable of running MATLAB autocode and operating on a wide power supply and temperature range. It is ideal for use in smaller more specific control applications and can also be used in conjunction with an optional Prodrive memory card to provide the functions of a versatile data logger at the same time as running the control system.

- 10 x Single ended analogue inputs
- 6 x digital inputs
- 8 x 2A low side drives
- 2 x 20mA analogue current outputs
- 2 x Internal accelerometers (2 axis in total)
- Internal temperature sensor
- Wide supply range
- Reverse and over-voltage protected
- Software compatibility with ProteusTM, MATLAB, Simulink, RTW and PippaTM

- Motorola MPC555 BlackOak microcontroller at 40 MHz
- PowerPC core with floating point unit
- 26Kb internal RAM, 448Kb of internal flash
- 512Kb SRAM
- 8Kb non-volatile FRAM (ideal for parameter storage)
- ProteusTM Synchronous Expansion Port
- Supports data logging capability via expansion connector
- Mating Connector: 37 way Filtered Autosport
- Robust case construction (IP67)

I/O specifications

Digital Inputs

Features:

- Protection against over-voltage up to 60V continuous.
- Protection against positive and negative transients
- Configurable (0-5V) threshold level
- Individual pull up, pull down and bias network configurations with 5 or 12 Volt options
- High impedance inputs
- Low pass filter with a nominal 10KHz cut off frequency

The digital inputs are single-ended and capable of accepting the outputs of numerous sensor types, e.g. hall effect, pressure switches etc.

Each digital input can be individually configured to trigger at a specific threshold value. The default values give a threshold of 2.5V.

All the digital inputs are connected to channels on the TPU this allows a wide range of signal types to be read automatically by the hardware TPU processor, e.g. discrete input, event time, and pulse time accumulator. The resolution of the input capture is determined by the software, the default setting is 4uS.

Analogue Inputs

Features:

- Protection against over-voltage up to 50 Volts
- Protection against positive and negative transients
- 2-pole bessel input filters (nominal cut off frequency 200Hz)
- Individual 5 volt pull up, pull down and bias network configurations.
- High impedance inputs

It is possible to customise the cut off frequency of each individual filter between 20 and 1000Hz by means of specific ECU configuration.

Internal Temperature sensor input

The ECU has an onboard internal temperature sensor. It covers the operating range of the ECU, plus some capability to detect heat-soak temperatures. The temperature range is 40°C to +100°C. The output of the sensor is read by an analogue channel on the CPU. This is performed internally and therefore does not require the use of an external analogue input channel.

Internal Accelerometers input

Features:

- Internally mounted
- 5g range
- Scalable range of 250mV/g to 1.5V/g where required FSD is less than 5g.
- Filtered output signal with hardware configurable cutoff (typically 200Hz).

Two single axis accelerometers are mounted at 90 degrees to one another. In this way the acceleration of the ECU can be measured in 2 axes. The accelerometers have 5mg resolution with range of 5g and a sensitivity of 250mV/g. The analogue cut-off frequency is set to 200Hz. The accelerometers are mapped onto two 10 bit analogue channels. This is performed internally and therefore does not require the use of external analogue input channels.

A gain of 1 to 6 (250-1500mV/g) can be hard configured depending on the customers needs.

DIGITAL OUTPUTS

All externally connected outputs are protected against automotive transients and steady state voltages.

Low side drives specifications:

- 2A nominal current handling per output
- 3A peak current handling per output
- 8A total permissible current across 8 outputs (100
- Switching of up to 45V sources.
- Current limiting
- Reverse EMF protection
- Ability to drive both resistive and inductive loads
- Over temperature protection

The UP100 supports eight low side drives with a nominal current handling capability of 2A. It is possible to switch up to 3A loads per channel provided that the total load across all eight channels is less than 8A. Each low side channel can sink voltages of up to 45V. The return path is separate to the supply ground of the unit allowing noise generated switching signals to be isolated from the unit.

Analogue outputs

Two analogue outputs are available, these can be configured as either a current or voltage drives. Current drives can be used to control Moog type hydraulic valves utilizing current feedback circuitry. Voltage drives provide an analogue voltage output, which can be used to drive circuits such as instrumentation packs

Current Output Specifications:

Output current:	$\mathbf{0 - 20}\boldsymbol{mA}$ or $\pm\mathbf{10}\boldsymbol{mA}$
DC resistance:	$\mathbf{500\Omega}$
Frequency range:	$\boldsymbol{dc\ to}\ \mathbf{50}\boldsymbol{Hz}$
Step Response:	$\mathbf{50}\boldsymbol{Hz}$

CUSTOMER CONFIGURATION

All the UP100s Digital and Analogue Inputs have a default configuration that can be customised upon request. Any customisation will be charged at extra cost and the customer configuration form is available upon request when the order is placed. Also additional features such as a data logging device are available upon request.

Processing hardware

The MPC555 is a high-speed 32-bit Central Processing Unit that contains a floating-point unit designed to accelerate the advanced algorithms necessary to support complex control applications. The CPU is ideal for high-performance data manipulation and coupled with a large on-chip FLASH memory with powerful peripheral subsystems allow for complete flexibility in the development process.

- 40MHz Core with Floating Point Unit
- 26KB of Static RAM
- 448KB Flash EEPROM Memory with 5V programming (CMF)
- Flexible Memory Protection Unit
- General purpose I/O Support
- Two Time Processor Units (TPU3)
- 10 channel PWM
- 8 channel double action units
- Two Queued Analog-to-Digital Converter Modules (QADC)
- Two CAN 2.0B Controller Modules (TouCANTM)
- Queued Serial Multi-Channel Module (QSMCM)
- 8Kb of non-volatile FRAM - allows users a permanent memory storage that is useful for storing settings and parameters required by the application or BIOS that may need to be changed frequently.
- 512Kb of SRAM application run-time memory space.

C.2 Servo motors

Based on specifications and availability two SAC55L60/0.5/TS/TB/CB/EY-2048 motors are used from Eltromat bv. These have the following specifications.

Stall torque	$\mathbf{0,8Nm}$
Cont torque	$\mathbf{0,5Nm}$
Max torque	$\mathbf{2Nm}$
U-bus	$\mathbf{48V}$
Max speed	$\mathbf{6000rpm}$
Cont current	$\mathbf{6.5A}$
Max current	$\mathbf{36A}$
Pn	$\mathbf{0,31kW}$
poles	$\mathbf{4p}$
Kt	$\mathbf{0,0769Nm/A}$
Kv	$\mathbf{137krpm/V}$
R	$\mathbf{0,135\Omega}$
I	$\mathbf{0,36mH}$
J	$\mathbf{0,02e-3kgm^2}$

C.3 Gear pumps

Two HPI pumps are bought at Koppen&Lethem for the pressure- and ratio pump: P3AAN0100FL20B01

Capacity	1 cc/rev
Max pressure	250 bar
Max speed	8000 rpm
Max flow	8 l/min
Weight	0.45 kg

C.4 Hall sensors

Hall sensors are bought at Farnell in ONE bv.

Type	1GT101DC
Supply voltage	4.5 - 24 Vdc
Supply current	10 mA typ, 20 mA max
Output voltage (low output)	0.4 V max
Output voltage (high output)	$\boldsymbol{V_{supply}}$
Output current (high output)	10 $\boldsymbol{\mu}$A max
Switch time rising	15$\boldsymbol{\mu}$sec max
Switch time falling	1.0 $\boldsymbol{\mu}$sec max

C.5 Pressure transducers

Two pressure transducers which are bought at Koppen&Lethem to measure primary and secondary pressure.

Type	KLPT-2221WH
Range	0-60 bar
Over pressure safety	120 bar
Burst pressure	550 bar
Supply voltage	5 Vdc
Signal output	0.5 - 4.5 Vdc
Response time	5ms max
Error	0.5 % (of span) max

C.6 Servo amplifiers

Two servo amplifiers are used from Eltromat bv.

Model	ASP-090-36
Peak output current	36 Adc / 25.5 Arms
Peak time	1 sec
Cont output current	12 Adc 8.5 Arms
Peak output power	2.95 kW
Cont output power	1.0 kW
Supply voltage	20 - 90 Vdc
Supply current peak	40 Adc
Supply current cont	13.3 Adc
Bandwidth current loop	3 kHz typical
Size	167*99*30 mm

C.7 DC-DC convertor

A DC-DC convertor has been built by TOP Systems BV which is suitable to charge 48 Vdc battery. This convertor has the following specifications.

Type	Orion 12/55-275
Input	9-18 Vdc
Output	55.2 Vdc
Charge current	5 A
Power	275 W
Forced cooling	yes
Galv seperation	yes
Efficiency	+85 %
Size (l*w*h)	49*177*182 mm
Norms Emission	EN 50081-1
Norms Immunity	EN 50082-1
Norms Automotive Directive	95/45/EC

Appendix D

EZL 799 Data sheet

A data sheet of EZL 799 oil, the oil which is being used in the Volvo transmission can be found on the next page. This sheet is made available Esso Lubricants and is only available in Dutch.

EZL 799

CVT vloeistof van het type Ford 166-H

BESCHRIJVING
EZL 799 is een vloeistof speciaal bestemd voor transmissies waar een Ford ESP-M2C 166-H kwaliteit voorgeschreven wordt.

TOEPASSING
Alle types automatische transmissies en meer in het bijzonder de CVT werkend volgens het Van Doorne's duwschakelband principe.

PRESTATIE
Kwaliteitsaanduiding
Ford ESP-M2C 166-H
Goedkeuringen
VDT

VOORDELEN
- Friction modified.
- Hoge oxidatiebestendigheid.
- Hoge thermische stabiliteit.
- Biedt bescherming tegen corrosie.
- Hoge viscositeitindex.
- Geringe neiging tot schuimvorming.
- Verdraagzaam ten opzichte van afdichtingmaterialen zoals toegepast in automatische transmissies.

TYPISCHE KENMERKEN	EENHEID	RESULTAAT	METHODE
Dichtheid bij 15 ºC	kg/m³	860	ASTM D 4052
Viscositeit bij -40 ºC	cSt	40 000	ASTM D 445
Viscositeit bij 18 ºC	cP	1300	ASTM D 2602
Viscositeit bij 40 ºC	cSt	39	ASTM D 445
Viscositeit bij 100 ºC	cSt	8	ASTM D 445
Viscositeitsindex		182	ASTM D 165
Vlampunt, COC	ºC	205	ASTM D 92
Zuurgetal, TAN	mg KOH/g	0.5	ASTM D 664
Kleur	-	rood	-
Koperstripcorrosie	(3h, 100ºC)	1	ASTM D 130
Corrosie test (+ = voldoet)		+	ASTM D 665A

GEZONDHEID & VEILIGHEID – Dit product is niet geclassificeerd als gevaarlijk onder de Europese Richtlijn inzake Gevaarlijke Stoffen en Preparaten. Nadere informatie op het Esso Veiligheidsinformatieblad.

ESSO Nederland B.V.
Postbus 1
NL-4803 AA BREDA
Tel.: 076-529 1300

ESSO Belgium, divisie van ESSO B.V.B.A./S.A.R.L.
Postbus 100
B-2060 ANTWERPEN 6
Tel.: (03) 226 27 74

augustus 2001

Transmissie olie

Product Data Sheet

Appendix E

Installing the servo system into the Volvo

A mount has been designed to connect the servo motors to the pumps. The design of this mount is shown in figure E.1. It is decided to lathe the mounts to ensure the axial alignment.

Initially a design based on an aluminum bracket was made to connect all the hydraulic parts. This design is shown in figure E.2. Since the aluminum bracket was leaking too much it is decided to keep all parts on the same position but to use piping to connect them.

In figure E.3 the placement of the primary and secondary pressure transducers and pressure gauges in the vehicle is shown. It is decided to use both a pressure transducer and a pressure gauge to be able to see the pressure as well as to measure it. The ratio servomotor can also be seen. These components are placed in front of the engine and transmission and behind the radiator.

In figure E.4 the placement of the pressure servo motor and pump are shown as well as the hall-sensor which measures the engine speed. The motor is placed at the side of the transmission at the bottom of the vehicle.

The 12-55 VDC convertor is shown in figure E.5 together with the four batteries and the required fusing. It is placed directly behind the front bumper next to the radiators.

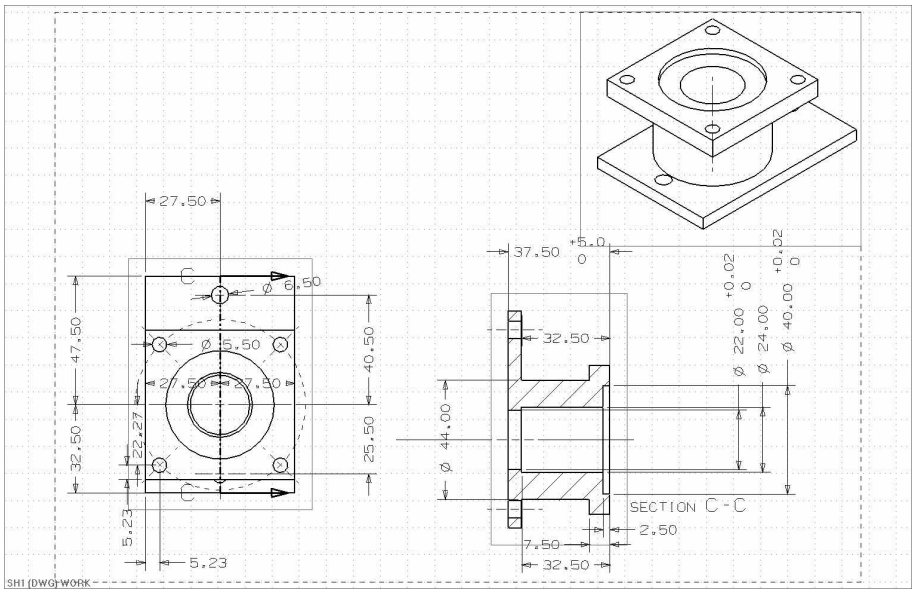

Figure E.1: The mount used to connect the pumps to the motors

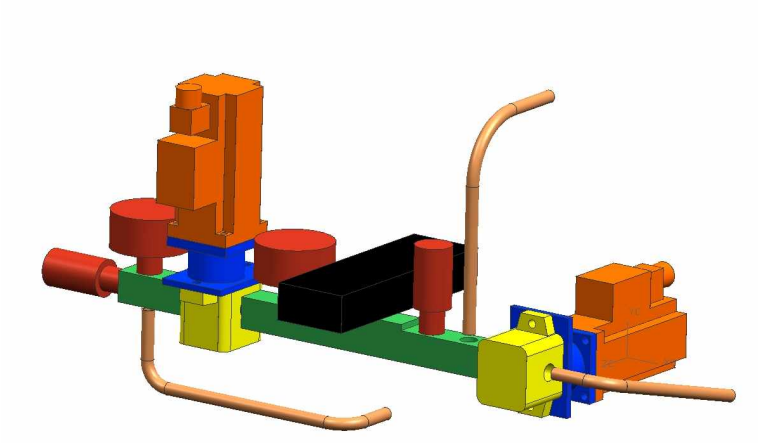

Figure E.2: The initial design to place the hydraulic system into the vehicle

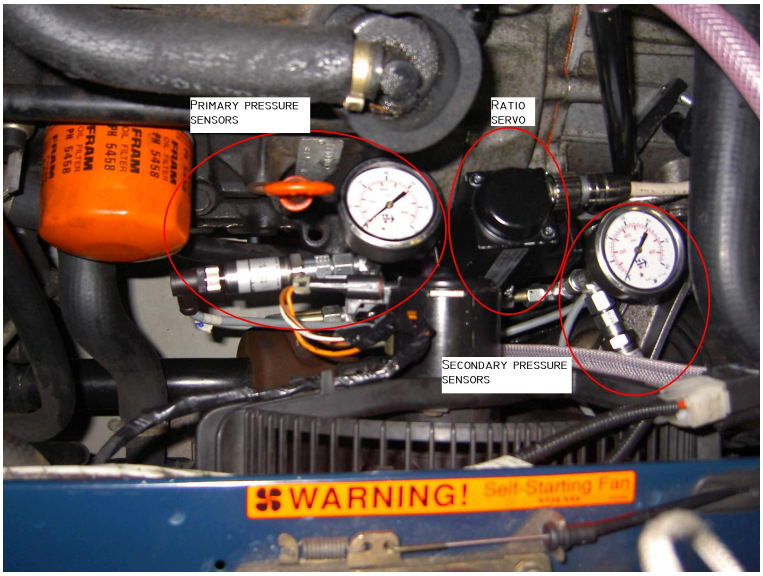

Figure E.3: The placement of pressure sensors and ratio servo between radiator and transmission

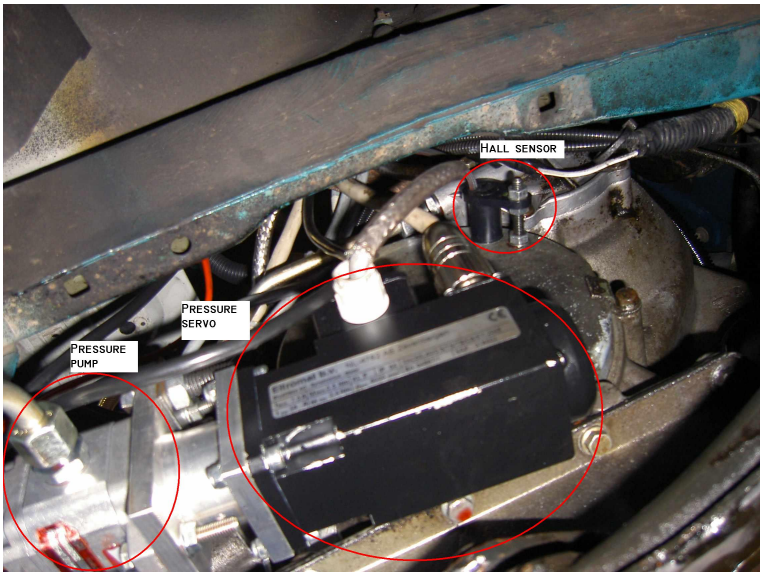

Figure E.4: The placement of pressure pump and servo and a hall-sensor at the bottom of the transmission

Figure E.5: The 12-55 VDC convertor in combination with four batteries between bumper and radiator

Appendix F

Leakage estimation

The measured leakage from the VT1-CVT is very high. Therefore, an estimation is made to see if this is correct. There are several leakage points, being the sealing between moving sheave and fixed sheave on both pulleys, the pressure compensation chamber at the secondary pulley and the oil inlet in both pulleys.

The movable sheave and the fixed shaft have a G7/h6 fit. Since the diameter is $\mathbf{45}\boldsymbol{mm}$ this means the shaft has a tolerance of $[\mathbf{+9 + 13}]\boldsymbol{\mu}$ and the pulleys $[\mathbf{0 - 16}]\boldsymbol{\mu}$. Thus the maximum gap height can be $\boldsymbol{h} = \mathbf{0.05}\boldsymbol{mm}$. The length of the sealing surface is $\boldsymbol{L} = \mathbf{10}\boldsymbol{mm}$ in low. The width of the gap is $\boldsymbol{b} = \mathbf{141}\boldsymbol{mm}$ (shaft circumference).

The leakage flow is given by:

$$\boldsymbol{Q} = \frac{\boldsymbol{\Delta p\, b\, h^3}}{\mathbf{12}\boldsymbol{\eta L}} \tag{F.1}$$

For a pressure difference of $\mathbf{10}\boldsymbol{bar}$ this results in a maximum leakage flow of about $\mathbf{90}\boldsymbol{cc/min}$.

The pressure compensation on the secondary pulley is fed by a small hole. Since the length of this hole is relatively small the flow can be approached by:

$$\boldsymbol{Q} = \boldsymbol{A}\, \boldsymbol{C_D} \sqrt{\frac{\mathbf{2}\boldsymbol{\Delta p}}{\boldsymbol{\rho}}} \tag{F.2}$$

$\boldsymbol{A} = \mathbf{3.9}\boldsymbol{e} - \mathbf{8}\boldsymbol{m^2}$ is the area of the hole and the constant $\boldsymbol{C_D} = \mathbf{0.6 - 0.7}$ depending on the sharpness of the edges of the hole. This leads to a leakage of approximately 80 cc/min.

Finally a leakage is possible on the oil inlet on the shaft. This is very difficult to calculate, since the quality of the sealing (after opening and closing several times) cannot be quantified. Since the total leakage at $\mathbf{10}\boldsymbol{bar}$ is about 1200 cc/min the leakage at the oil inlets has to be roughly 1030 cc/min. This is extremely high.

Based on these rough calculations it is expected that there is an unknown leakage somewhere in the CVT which has to be compensated by the pressure pump.

It turned out that the oil channel, which was made into the housing of the transmission to pressurize the primary pulley was leaking. The oil pressure was slowly pressing out a plug. This leakage has been fixed and the leakage of the transmission was measured again.

Appendix G

Pump measurements

G.1 Generated pressure

In figure 4.9 the generated pressure is shown as a function of commanded current through the servo motor. During the proces of tuning the pressure controller the maximum pressure which could be reached dropped all of a sudden. In figure G.1 the same measurements as in figure 4.9 are shown as well as the new relation between the commanded current and the generated pressure.

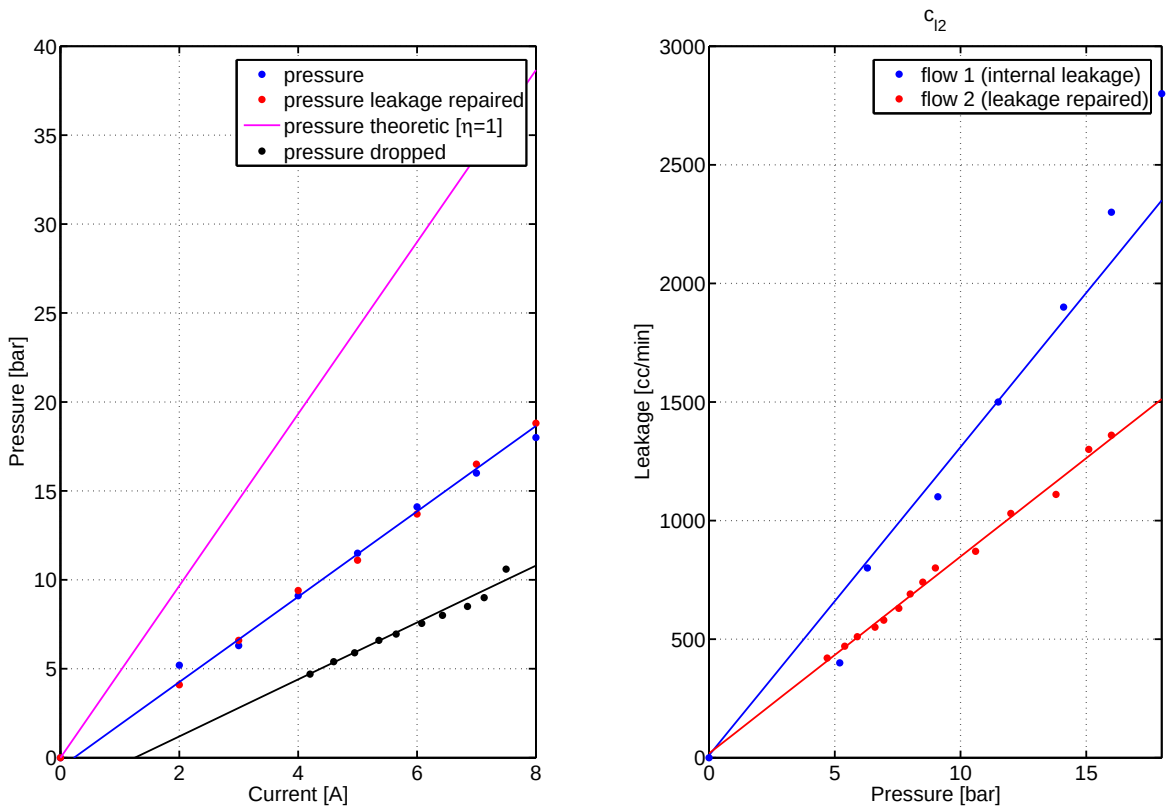

Figure G.1: The limited pressure created by the pump

It can be seen that the static friction all of a sudden is very high. There is a current of $\mathbf{1.5}\boldsymbol{A}$ needed to start generating a pressure. This is already one fifth of the maximum continuously available current. Beside that the efficiency of the pump became worse. A possible explanation is that large particles are stuck between the gears of the pump and the housing causing the pump to create more friction. These particles can also cause the efficiency of the pump to drop when they grind down the housing or the gears. Due to time limitations it is not possible to investigate the cause of this limitation any further. To continue with this project the pump has to be removed and a thorough investigation to the cause of the changed friction and efficiency has to performed.

G.2 Power consumption

In section 4.9 the power consumption of the entire servo system is discussed both in the real situation as in the case if there would be less leakage. The individual power consumption of both servo motors for the present situation is shown in figures G.2 and G.3. The entire power consumption is shown in figure G.4 (same as figure 4.20).

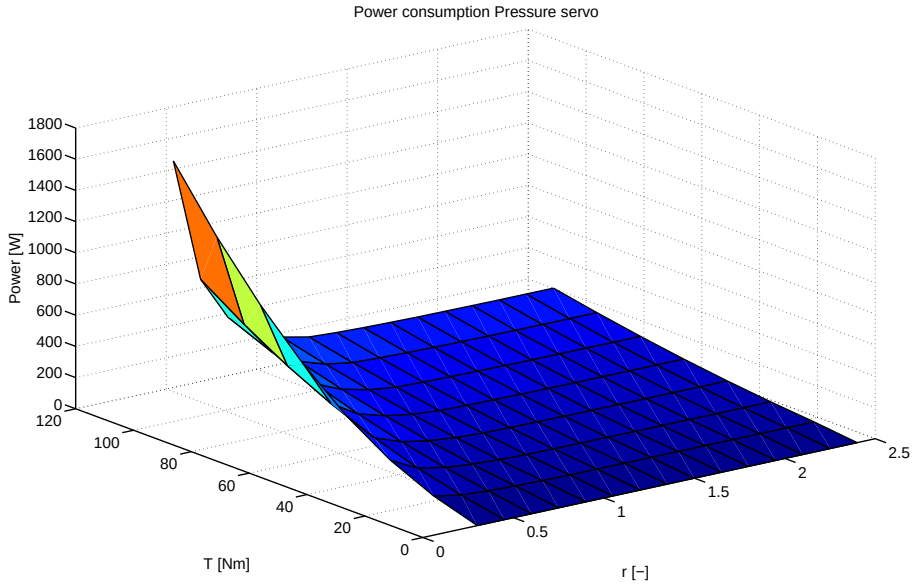

Figure G.2: The power consumption of the pressure-servo motor.

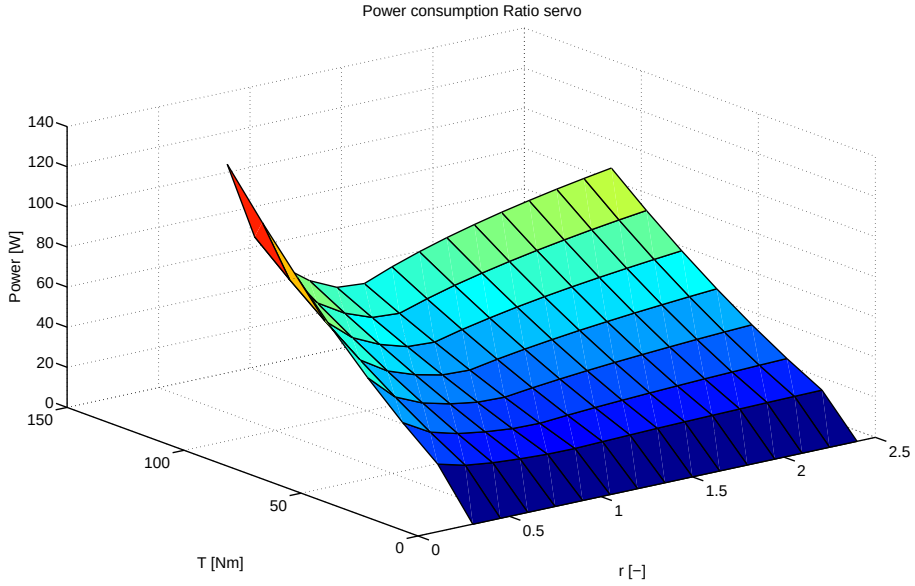

Figure G.3: The power consumption of the ratio-servo motor.

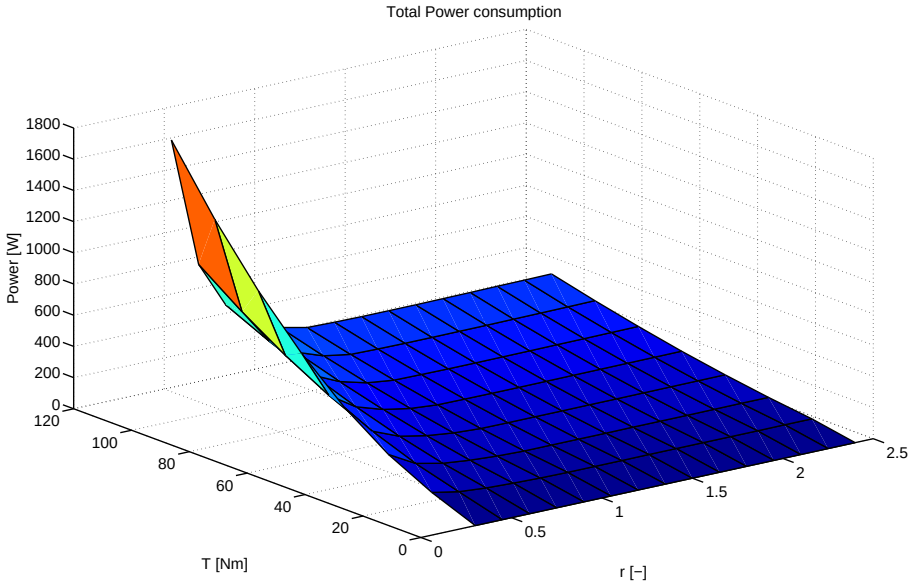

Figure G.4: The power consumption of the servo system in the Volvo VT1.

Appendix H

Diagrams of the controlled system

In section 4.7 a controller is designed for the secondary pressure circuit. In this appendix the Bode diagrams of the system on it self, the controller, the open loop, the sensitivity, the Nyquist diagram and the the closed loop are shown.

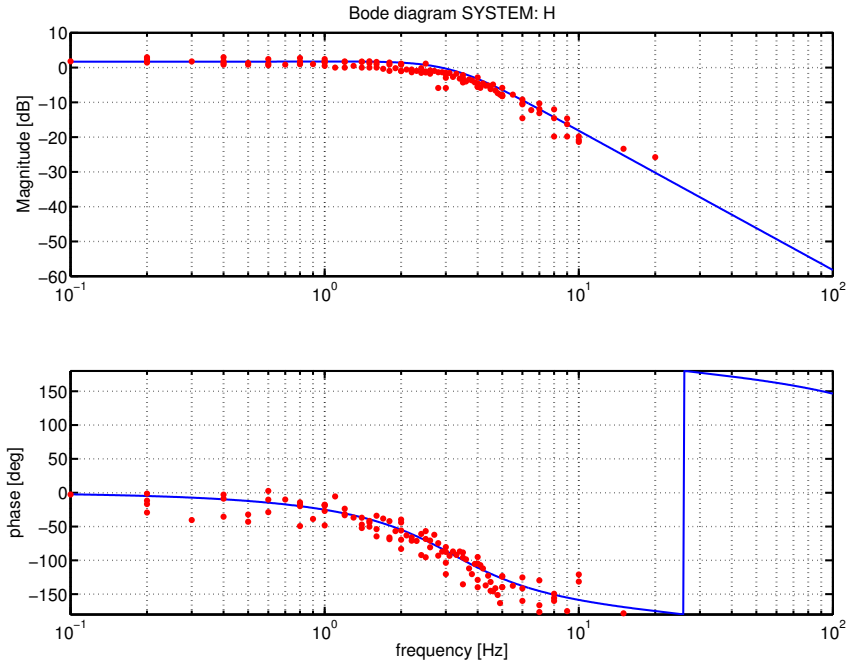

Figure H.1: The measured and fitted bode diagram of the secondary oil circuit of the VT1 CVT in LOW ratio

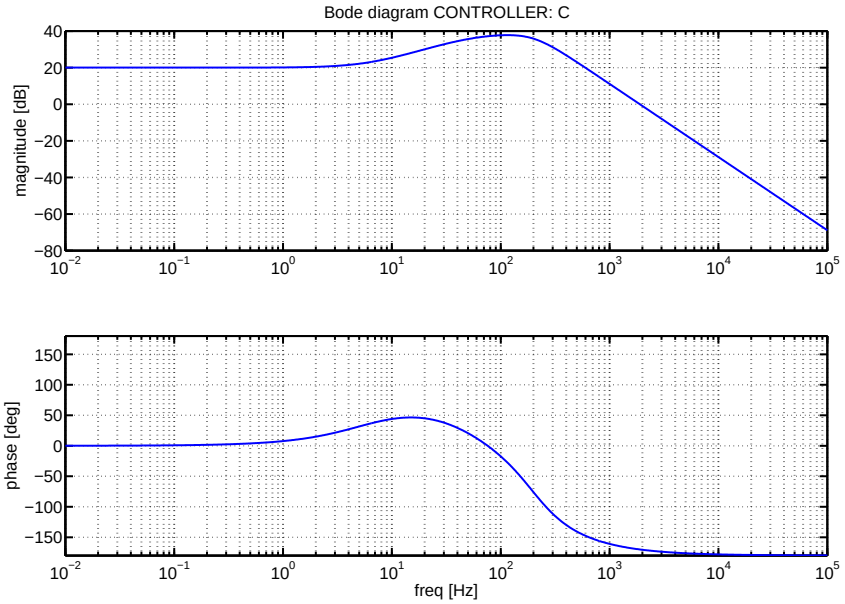

Figure H.2: The bode diagram of the controller

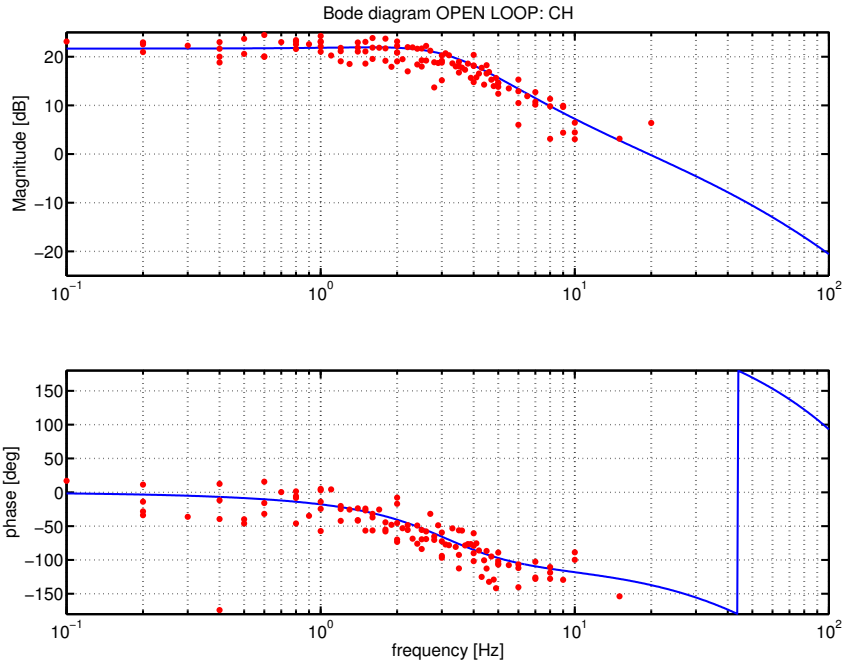

Figure H.3: The bode diagram of the open loop system

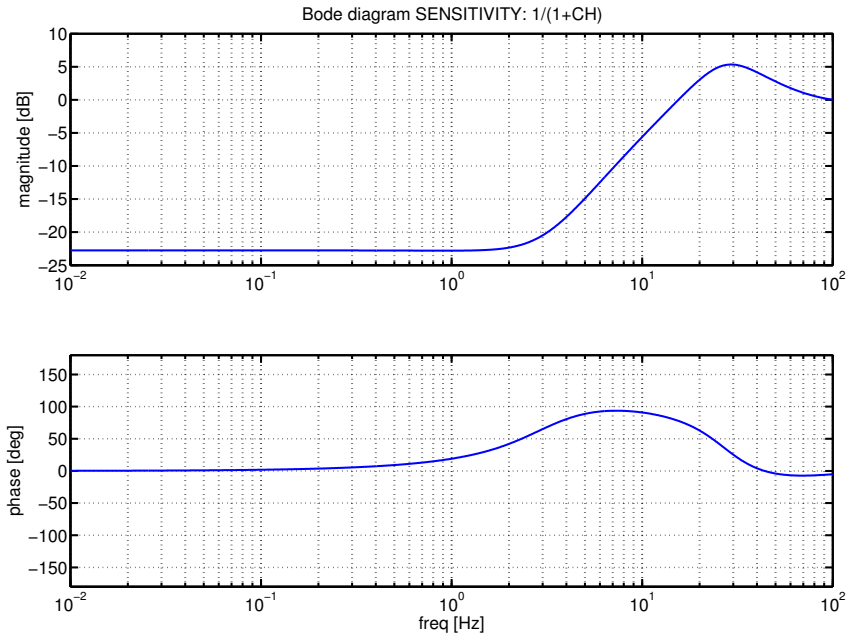

Figure H.4: The bode diagram of the sensitivity

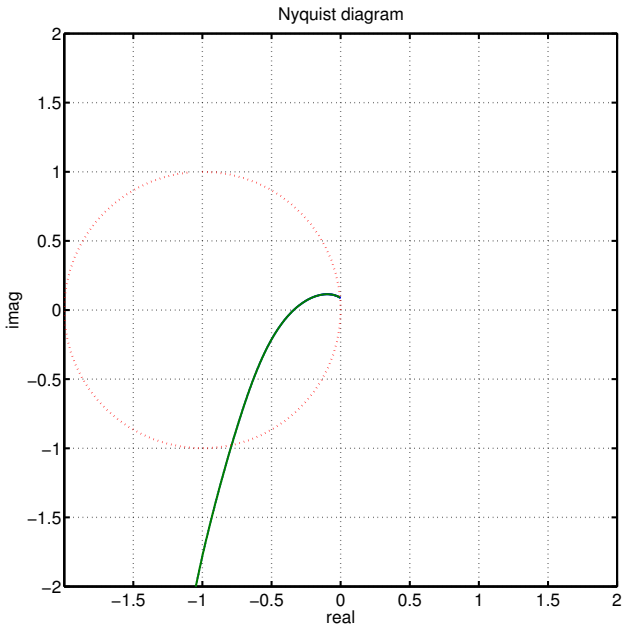

Figure H.5: The Nyquist diagram of the system

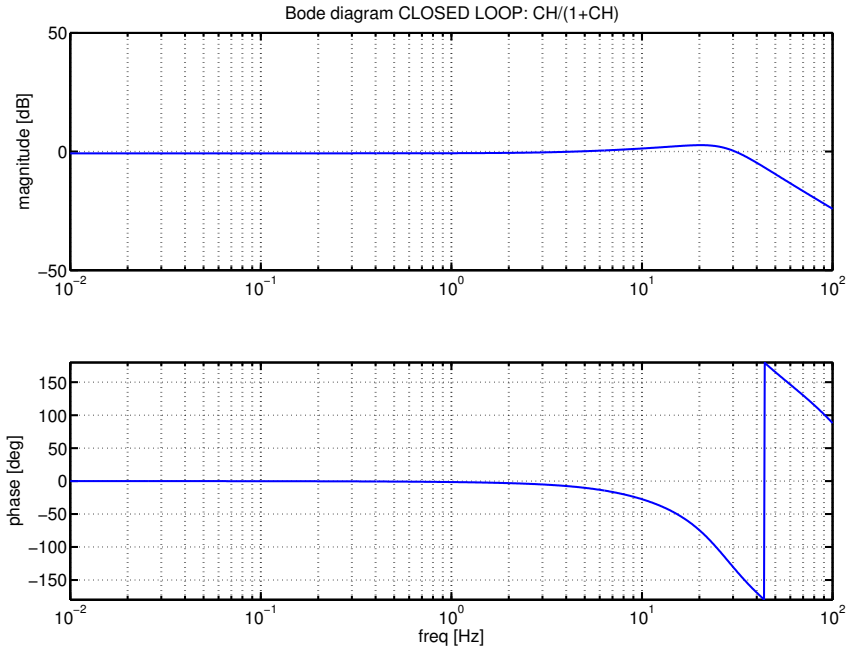

Figure H.6: The bode diagram of the closed loop system

Bibliography

[ABC+04] A. Allen, C. Bangar, T. Carde, D. Dalal, A. Frank, and J. Garar, *Design and development of the 2004 UC Davis Future Truck*, Tech. report, University of California, Davis, 2004.

[Ake01] Sam Akehurst, *An investigation into the loss mechanisms associated with a pushing metal v-belt cvt*, Ph.D. thesis, University of Bath, 2001.

[BGM72] Jean J. Botti, M. James Grieve, and John A. MacBain, *Electric vehicle range extension using an SOFC APU*, SAE Technical Paper Series (2005-01-1172).

[Bra03] Thomas H. Bradley, *Simulation of continuously variable transmission chain drives with involute inter-element contact surfaces*, Master's thesis, University of California, Davis, 2003.

[CJW55] Paul Cook, Peter James, and Mark Willows, *Rapid prototyping of generic hybrid concept vehicles*, SAE World Congress (2002-01-0755).

[FBvR04] A.A. Frank, A.W. Brown, and J.H.H. van Rooij, *The design of an inline GCI chain CVT for large vehicles*, International Continuously Variable and Hybrid Transmission Congress, September 2004.

[Fra04a] A.A. Frank, *Engine optimization concepts for CVT-Hybrid systems to obtain the best performance and fuel efficiency*, International Continuously Variable and Hybrid Transmission Congress, September 2004.

[Fra04b] Andrew A. Frank, *Compact inline longitudinal CVT; patent no:WO-2005/032873-A2*, September 2004.

[IUK96] T. Ide, H. Uchiyama, and R. Kataoka, *Model of a continuously variable transmission*, JSAE (1996), no. 9636330.

[Jam04] Peter James, *Mechatronics and automotive design*, International Journal of Electrical Engineering Education (2004).

[Lab01] National Renewable Energy Laboratory (ed.), *Joint advisor/psat vehicle systems modeling user conference*, 2001.

[Nel03] Joost Nelissen, *Power loop test rig, variator redesign and development of a power loop test rig.*, Dct-2003/20, Technische Universiteit Eindhoven, 2003.

[Pro03] ProDrive, ***µ****proteus up100 ecu detailed specifications*, September 2003.

[Sha04] Siddharth Shastri, *Comparison of energy consumption and power losses of a conventionally controlled cvt with a servo-hydraulic controlled cvt and with a belt and chain as the torque transmitting element*, International Continuously Variable and Hybrid Transmission Congress, 2004.

[vR] Jaques van Rooij, *Clamping force theory*, Internal publication.

[W+01] J.P. Wallace et al., *Well-to-wheel energy use and greenhouse gas emissions of advanced fuell/vehicle systems; north american analysis*, Tech. report, GMC, Argonne, BP, ExxonMobil, Shell, 2001.

[Win] URL: `http://www.windriver.com/`.

List of Figures

Acknowledgement

Initially I planned to do an internship at the University of California for half a year. Due to difficulties with obtaining a visa I decided to do my internship in The Netherlands and to do a part of my Masters Project at UC-Davis. This project was done in cooperation with Gear Chain Industrial where I worked on the second part of this project.

I would like to thank prof. Frank for giving me the possibility to work at the HEV-center for half a year. The ever continuing discussions during our lunch breaks were very stimulating and educational. Also many thanks to Leonhard Fahredin, Tashari El Sheik and Siddarth Shastri for the very pleasant work atmosphere in and outside our office. Thanks to Bill Brown for making the housing of the transmission and driving 800 km to bring it to 'us guys', just to make sure everything arrived all right. Also many thanks to Joost Nelissen, my colleague at GCI and my two supervisors, Jacques van Rooij from GCI and Bas Vroemen from the TU/e. Thans to Mark Willows for receiving us in England and his help with the controller. Finally I would like to thank all those people who gave me advice with the practical issues I had to overcome: Mike and Leo from the machine-shop in UC-Davis and Erwin, Wietse, Ruud and Toon from the lab in Eindhoven.

Samenvatting

De University of California in Davis heeft een batterij dominant, parallel, plug-in hybride voertuig gemaakt. Om de mogelijkheden van deze hybride aandrijf lijn volledig te benutten is besloten de handmatige transmissie te vervangen door een Continu Variabele Transmissie. Hiervoor moest een nieuw soort CVT ontwikkeld worden en de power train controller van het voertuig moest worden aangepast. De CVT zal aangestuurd worden door middel van een servo-hydraulisch controle systeem. Om ervaring op te doen met dit systeem is het ingebouwd in een ander voertuig.

Het eerste hoofdstuk van dit verslag behandeld verschillende type hybride voertuigen in het algemeen en de hybride gemaakt door UC-Davis in het bijzonder. Er wordt verklaard waarom bepaalde beslissingen zijn genomen die tot het huidige ontwerp hebben geleidt. De volgende stap in de ontwikkeling van dit voertuig is het vervangen van de manuele transmissie door een CVT. De voordelen van een CVT en de noodzakelijke power train controller zullen worden besproken. Het tweede hoofdstuk behandeld de nieuwe transmissie, de inline CVT, die speciaal voor dit voertuig is ontworpen. Het karakteristieke gedrag en de verschillen met een conventionele CVT worden uitgelegd. De inline CVT zal worden aangestuurd met een servo-hydraulisch actuatie systeem, omdat dit systeem naar verwachting minder vermogen nodig heeft om de CVT aan te sturen in vergelijking met een conventioneel actuatie systeem. De theorie van dit systeem zal worden besproken in hoofdstuk drie. Om ervaring op te doen met het actuatie systeem is het ingebouwd in een voertuig. Alles wat hiervoor nodig is en hoe dit is gedaan wordt beschreven in hoofdstuk 4. Tot slot zal het model worden vergeleken met meetingen die aan het voertuig zijn gedaan.

Nomenclature

Acronyms

Some of the acronyms explained here are not used in this report, but are used in the ProDrive UP100 software.

Acronym	Description
APU	Auxiliary Power Unit
CAN	Control Area Network
CD	Charge Depletion
CS	Charge Sustaining
CVT	Continuous Variable Transmission
EM	Electric Motor
EMF	Electro Mechanical Force
EPRI	Electric Power Research Institute
EV	Electric Vehicle
GCI	Gear Chain Industrial bv
HEV	Hybrid Electric Vehicle
HEV-center	Hybrid Electric Vehicle center of UC-Davis
HVAC	Heating, Ventilation and Air Conditioning
ICE	Internal Combustion Engine
IOL	Ideal Operating Line
LED	Light Emitting Diode
MDASM	MIOS Double Action Submodule
MIOS	Modular IO System
MPWM	MIOS Pulse Width Modulation Submodule
PSAT	A Matlab 'Powertrain System Analysis Toolkit' developed by Argonne National Laboratory
QADC	Queued Analog-to-Digital Converter
RMS	Root Mean Square value
SCI	Serial Communications Interfaces
SOC	State of Charge of a battery

Acronym	Description
SULEV	Super Ultra Low Emission Vehicle
SUVs	Sport Utility Vehicles
TPU	Time Processing Unit
TTW	Tank to Wheel emissions
TU/e	Eindhoven University of Technology
UC-Davis	University of California, Davis
US	United States
WTT	Well to Tank emissions
WTW	Well to Wheel emissions

Symbols

Symbol	Description	Value	Unit
α_{road}	road angle		rad
α_{steel}	thermal expansion coefficient of steel	$1.24e-5$	$°C^{-1}$
β	angel of a pulley sheave	$0,19$	rad
η_m	mechanical pump efficiency		$-$
η_v	volumetric pump efficiency		$-$
μ	dynamic viscosity = $\nu \cdot \rho_{oil}$	$0,1$	Ns/m^2
ν	kinematic viscosity	$0,125e^{-3}$	m^2/s
ρ_{air}	density of air	$1,2$	kg/m^3
ρ_{oil}	density of oil	860	kg/m^3
ω_1	speed of primary drive train		rad/s
ω_2	speed of secondary drive train		rad/s
ω_p	speed of pressure pump		rad/s
ω_r	speed of ratio pump		rad/s
a	center distance between two pulleys		m
c_{l1}	leakage coefficient for primary circuit		m^5/Ns
c_{l2}	leakage coefficient for secondary circuit		m^5/Ns
c_d	drag coefficient of the vehicle		$-$
c_p	pump displacement	$1e^{-6}/2\pi$	m^3/rad
c_s	static friction coefficient		N
c_v	dynamic friction coefficient		N/rad
d	pipe diameter		m/s
f_{rol}	coefficient of rolling resistance		$-$

Symbol	Description	Value	Unit
a	center distance between two pulleys		m
c_{l1}	leakage coefficient for primary circuit		m^5/Ns
c_{l2}	leakage coefficient for secondary circuit		m^5/Ns
c_d	drag coefficient of the vehicle		$-$
c_p	pump displacement	$1e^{-6}/2\pi$	m^3/rad
c_s	static friction coefficient		N
c_v	dynamic friction coefficient		N/rad
d	pipe diameter		m/s
f_{rol}	coefficient of rolling resistance		$-$
g	gravitational constant	$9,81$	m/s^2
m	mass of the vehicle		kg
p	pressure		Pa
p_1	pressure in primary circuit		Pa
p_2	pressure in secondary circuit		Pa
Δp_p	pressure difference pressure pump		Pa
Δp_r	pressure difference ratio pump		Pa
r	ratio $=\frac{\omega_2}{\omega_1}$		$-$
$\dot{r}$	ratio rate $=\frac{dr}{dt}$		$1/s$
r_I	ratio of 'first' CVT of inline CVT		$-$
r_{II}	ratio of 'second' CVT of inline CVT		$-$
v	vehicle speed		m/s
v_{oil}	oil speed		m/s
Δx	stroke of a movable pulley		m
A_{front}	frontal area of the vehicle		m^2
D_0	original diameter		m
ΔD	change in diameter		m
E_b	bulk modulus	$1e^9$	N/m^2
F_1^*	clamping force required to maintain ratio		N
F_{cent}	centrifugal force		N
F_{cli}	climbing resistance		N
F_{dra}	drag resistance		N
F_{in}	clamping force on 'input' pulley		N
F_{out}	clamping force on 'output' pulley		N
F_{RL}	road load force		N
F_{rol}	rolling resistance		N
I_p	current through pressure-servomotor		A
I_r	current through ratio-servomotor		A
J_1	moment of inertia of the primary drive train		kg/m^2
J_2	moment of inertia of the secondary drive train		kg/m^2
J_m	moment of inertia motor	$0,02e^{-3}$	kg/m^2
J_p	moment of inertia pump	$0,005e^{-3}$	kg/m^2
K_t	motor constant	$0,0769$	Nm/A

Symbol	Description	Value	Unit
K_v	EMF constant	**0.0459**	Vs/rad
L	length of the CVT chain		m
P_{RL}	road load power		W
Q	flow		m^3/s
Q_{l1}	flow leaking out of primary circuit		m^3/s
Q_{l2}	flow leaking out of secondary circuit		m^3/s
Q_1	flow into primary circuit		m^3/s
Q_2	flow into secondary circuit		m^3/s
Q_p	flow through pressure pump		m^3/s
Q_r	flow through ratio pump		m^3/s
$R_{[1:4]}$	running radius on pulley 1 till 4 (of inline CVT)		m
R_{id}	inner radius of piston		m
R_{in}	running radius at input pulley		m
R_{od}	outer radius of piston		m
R_{out}	running radius at output pulley		m
R_0	running radius at ratio 1		m
R_m	electrical resistance motor	$\mathbf{0,135}$	Ω
ΔR	change in running radius		m
$T_{drive-shaft}$	drive shaft torque		Nm
T_{EM}	electric motor torque		Nm
T_{ICE}	engine torque		Nm
T_{mp}	torque generated by pressure-servomotor		Nm
T_{mr}	torque generated by ratio-servomotor		Nm
T_p	torque generated by pressure pump		Nm
T_r	torque generated by ratio pump		Nm
ΔT	temperature difference		$°C$
V_{2_0}	minimum volume secondary circuit		m^3
V_2	secondary volume		m^3
ΔV_2	change of volume secondary circuit		m^3